Available online at www.sciencedirect.com

SciVerse ScienceDirect

Geochimica et Cosmochimica Acta 75 (2011) 6780–6802

Geochimica et Cosmochimica Acta

www.elsevier.com/locate/gca

A new approach to the equation of state of silicate melts: An application of the theory of hard sphere mixtures

Zhicheng Jing [a,b,*], Shun-ichiro Karato [b]

[a] Center for Advanced Radiation Sources, The University of Chicago, Argonne, IL 60439, USA
[b] Department of Geology and Geophysics, Yale University, New Haven, CT 06520, USA

Received 26 January 2011; accepted in revised form 29 August 2011; available online 8 September 2011

Abstract

A comparison of compressional properties of silicate solids, glasses, and liquids reveals the following fundamental differences: (1) Liquids have much smaller bulk moduli than solids and glasses and the bulk moduli of various silicate melts have a narrow range of values; (2) Liquids do not follow the Birch's law of corresponding state as opposed to solids and glasses; (3) The Grüneisen parameter increases with increasing pressure for liquids but decreases for solids; (4) The radial distribution functions of liquids show that the interatomic distances in liquids do not change upon compression as much as solids do. The last observation indicates that the compression of silicate melts occurs mostly through the geometrical arrangement of various units whose sizes do not change much with compression, i.e., the entropic mechanism of compression plays a dominant role over the internal energy contribution. All of the other three observations listed above can be explained by this point of view. In order to account for the role of the entropic contribution, we propose a new equation of state for multi-component silicate melts based on the hard sphere mixture model of a liquid. We assign a hard sphere for each cation species that moves in the liquid freely except for the volume occupied by other spheres. The geometrical arrangement of these spheres gives the entropic contribution to compression, while the Columbic attraction between all ions provides the internal energy contribution to compression. We calibrate the equation of state using the experimental data on room-pressure density and room-pressure bulk modulus of liquids. The effective size of a hard sphere for each component in silicate melts is determined. The temperature and volume dependencies of sphere diameters are also included in the model in order to explain the experimental data especially the melt density data at high pressures. All compressional properties of a silicate melt can be calculated using the calibrated sphere diameters. This equation of state provides a unified explanation for most of compressional behaviors of silicate melts and the experimental observations cited above including the uniformly small bulk moduli of silicate melts as well as the pressure dependence of Grüneisen parameters. With additional data to better constrain the key parameters, this equation of state will serve as a first step toward the unified equation of state for silicate melts.

1. INTRODUCTION

Compressional properties of silicate melts including density and its pressure (or temperature) derivative, i.e., bulk modulus (or thermal expansivity), are crucial to our understanding of many geological problems such as the generation and differentiation of silicate melts in the Earth's mantle, and the evolution of a melt layer (e.g., the putative magma ocean) in a planet. Important issues in this regard include the density of melts with various chemical compositions under deep Earth conditions (i.e., equation of state (EOS)) and the variation of some thermodynamic properties such as the Grüneisen parameter with compression. In order to understand these issues, a physically sound model is needed for the compression of molten materials under deep Earth conditions.

* Corresponding author at: Center for Advanced Radiation Sources, The University of Chicago, Argonne, IL 60439, USA. Tel.: +1 630 252 0435; fax: +1 630 252 0436.
E-mail addresses: zjing@uchicago.edu, jing@cars.uchicago.edu (Z. Jing).

0016-7037/$ - see front matter © 2011 Elsevier Ltd. All rights reserved.
doi:10.1016/j.gca.2011.09.004

However, unlike the solid and gaseous states of a matter for which there are widely accepted idealized models such as a crystal lattice and an ideal gas, describing the properties of liquids is challenging because they are nearly as dense as solids yet there is no long-range order in atomic positions (see textbooks, e.g., Egelstaff, 1994; March and Tosi, 2002; Barrat and Hansen, 2003; Hansen and McDonald, 2006). In the past, purely empirical equations of state were frequently employed for silicate melts. One such type of EOS is the Taylor expansion of volume in terms of pressure (e.g., Lange and Carmichael, 1987, 1990; Kress and Carmichael, 1991). The effect of liquid composition on volume is studied by the ideal mixing model first developed by Bottinga and Weill (1970). In the Bottinga–Weill model, the molar volume of a melt is a linear function of the partial molar volume of each oxide component (SiO_2, for example) in the melt, implying that the compression of a complex liquid can be modeled as a sum of the compression of individual solid-like component. Similarly, higher order coefficients in the Taylor expansion are calculated from properties of oxide components by assigning bulk modulus for each component oxide (e.g., Lange and Carmichael, 1987). This type of approach was employed in the widely used software package MELTS (Ghiorso and Sack, 1995) for the modeling of phase equilibria in magmatic systems. Apart from the obvious limitation that such an approach works only to a low degree of compression (Lange and Carmichael, 1987), there is a fundamental issue for the basic concept behind this approach: An implicit assumption is that the compression of a complex liquid such as a silicate melt can be viewed as the weighted average of compression of individual oxide components. As we will show in this paper, existing data on bulk moduli and radial distribution functions of silicate melts suggest that such a solid-based model of compression is unlikely valid for the compression of silicate melts.

A modified version of a curve-fitting approach has recently been proposed by Ghiorso and his co-worker (Ghiorso, 2004a,b,c; Ghiorso and Kress, 2004) using the Padè approximation. In this approach, some complications such as the influence of mixing of SiO_2 species with different Si–O coordination numbers are included. However, this is again an entirely empirical approach and the formula used in their approach has no strong physical basis.

Another group of equations of state borrows directly the ideas developed for solids. These include the widely used third-order Birch–Murnaghan EOS (Birch, 1947) and the Vinet EOS (Vinet et al., 1986). Many studies for silicate liquids at high pressure employ the Birch–Murnaghan EOS (e.g., Rigden et al., 1989; Agee, 1998; Stixrude and Karki, 2005). Also, it was utilized in pMELTS (Ghiorso et al., 2002), the revised version of MELTS, for the modeling of phase equilibria up to 3 GPa. Similarly, Stixrude and Karki (2005) explained the calculated trend in Grüneisen parameter using the behavior of Grüneisen parameters of the corresponding solids. The physical basis for the Birch–Murnaghan EOS is that the thermodynamics of a given material is completely characterized by the volumetric strain and that the influence of temperature can be included through the temperature dependence of parameters such as bulk modulus. Such an approach is valid when the major contribution to the free energy is the internal energy. However, as we will demonstrate in this paper, several observations strongly suggest that it is not the internal energy that changes most upon compression of a silicate melt: the factor that plays the most important role in the compression of silicate melts is entropy. In these cases, concepts borrowed from solids may not be applied to liquids.

The modern theories of liquids (see textbooks, e.g., Hansen and McDonald, 2006) may provide a more promising way to obtain the EOS for silicate liquids. These theories relate the microscopic description of atomic configurations and interactions in liquids to thermodynamic properties with the help of classical statistical mechanics. The key to this approach is to make adequate approximations for the interatomic potentials of atoms (and/or ions) and the correlation functions of atomic configurations. Among various equations that have been proposed (Hansen and McDonald, 2006), a simple but widely used equation is the hard sphere equation of state (Reiss et al., 1959; Thiele, 1963; Wertheim, 1963), which successfully calculates the entropic contribution through the excluded volume effect of rigid molecules in liquids. As we will show in this paper, the hard sphere EOS can naturally explain some of the most distinct compressional behaviors of silicate liquids. Guillot and Sarda (2006) first applied the hard sphere EOS to describe the compression of some silicate melts such as peridotitic and basaltic melts up to 10 GPa, demonstrating the applicability of the hard sphere EOS to silicate melts. However, their approach cannot be applied to study the effect of melt composition since the silicate melt was treated as a single component system with an average sphere diameter defined for all melt components. A more critical problem is that the hard sphere EOS oversimplifies the interatomic potential between atoms by neglecting the cohesion energy of liquids, which results in an infinite molar volume at zero pressure. Therefore the EOS had to be scaled to a reference data point in Guillot and Sarda (2006) to obtain the hard sphere diameter. In order to describe more realistic ionic liquids with Coulombic interactions, many charged hard sphere mixture models (e.g., Caccamo and Malescio, 1989; Blum et al., 1992; Rosenfeld, 1993) have been developed using statistical mechanics in the liquid state physics literature. Despite the sophisticated formulations of these models, which often involve integral equations, the application of these models are often limited to simple cases such as binary mixtures with equally sized and charged ions, i.e., the restricted primitive model (e.g., Blum et al., 1992; Fisher and Levin, 1993; Zhou and Stell, 1995; Zhou et al., 1995; Guillot and Guissani, 1996). Since the purpose of this paper is to develop a simple model for the equation of state of complex silicate liquids that can be readily used for geochemical and geophysical modeling, we choose an alternative approach by modifying the model of hard sphere mixtures (Lebowitz, 1964; Lebowitz et al., 1965; Mansoori et al., 1971) using some empirical approximations for the Coulombic potential energy and soft repulsion between spheres to account for the experimental data of silicate liquids.

In this paper, we will first review the experimental (and computational) observations on the compressional properties of silicate liquids, solids, and glasses and discuss the differences in the compressional behaviors of these states. We will show that these differences can be explained by the important contribution of entropy as opposed to internal energy. We will then propose a new equation of state for silicate liquids that provides a unified explanation for all the observations based on the modified hard-sphere model of liquids, which emphasizes the entropic contribution to compression.

2. A REVIEW OF OBSERVATIONS ON COMPRESSIONAL PROPERTIES

2.1. Comparison of density and bulk modulus

If temperature (T) and volume (V, see Table 1 for the definition of symbols) are chosen as the independent variables, then the isothermal EOS of a material can be given by the volume derivative of the Helmholtz free energy (F) of the material as,

$$P = -\left(\frac{\partial F}{\partial V}\right)_T = -\left(\frac{\partial U}{\partial V}\right)_T + T\left(\frac{\partial S}{\partial V}\right)_T, \quad (1)$$

which contains both the internal energy contribution and the entropy contribution. The second-order volume derivative of free energy (F) gives the isothermal bulk modulus

$$K_T = -V\left(\frac{\partial P}{\partial V}\right)_T = V\left(\frac{\partial^2 U}{\partial V^2}\right)_T - TV\left(\frac{\partial^2 S}{\partial V^2}\right)_T, \quad (2)$$

which also has two contributions.

Fig. 1 compares the density and bulk modulus of silicate liquids and solids with the same compositions at room pressure. We can see that the densities of silicate liquids are only slightly smaller (by 10–20%) than those of the corresponding solids, whereas the bulk moduli of silicate liquids are much smaller (a factor of 3–6) than those of their solid counterparts. Therefore the large difference in bulk moduli between liquid and solid silicates is not due to the difference in density. That is, the compression of silicate liquids does not follow the Birch's law of corresponding state (e.g., Birch, 1961; Anderson and Nafe, 1965; Chung, 1972; Shankland, 1972) (for more details on Birch's law see Appendix A). It should also be noted that the bulk moduli of silicate liquids have a relatively narrow range (17–27 GPa for the liquids plotted) in contrast to the corresponding solids (56–134 GPa).

Additional information on compression mechanisms can be gathered by comparing the bulk modulus as a function of density (or molar volume) for a given composition in different states (liquid, glass, and solid). Fig. 2 plots the bulk moduli of solid, glass and liquid states of $CaMgSi_2O_6$ (diopside or Di), $CaAl_2Si_2O_8$ (anorthite or An), and $NaAlSi_3O_8$ (albite or Ab) as a function of molar volume per atom. It is clear that the data of glasses and crystalline

Table 1
Definition of symbols used in the text.

Symbol	Definition	Units
$\overline{M}$	Molar mass (molar formula weight)	kg mol^{-1}
$\overline{V}$	Molar volume	m^3 mol^{-1}
n	Number of atoms per formula	–
$\overline{M}_a = \overline{M}/n$	Mean atomic weight	kg mol^{-1}
$K_T = -V(\partial P/\partial V)_T$	Isothermal bulk modulus	Pa
$\alpha = (\partial V/\partial T)_P/V$	Thermal expansivity	K^{-1}
$C_V = T(\partial S/\partial T)_V$	Constant volume specific heat	J K^{-1} mol^{-1}
$C_P = T(\partial S/\partial T)_P$	Constant pressure specific heat	J K^{-1} mol^{-1}
$\gamma = \alpha K_T V/C_V$	Grüneisen parameter	–
$(\partial K_T/\partial T)_V/\alpha K_T$	Intrinsic temperature dependence of bulk modulus	–
$K'_T = -(\partial \ln K_T/\partial \ln V)_T$	Pressure derivative of bulk modulus	–
$\delta_T = -(\partial \ln K_T/\partial \ln V)_P$	Anderson–Grüneisen parameter	–
$\chi = -(\partial \ln K_T/\partial \ln V)_{\overline{M}_a}$	Volume derivative of K_T at constant $\overline{M}_a$	–
$q = (\partial \ln \gamma/\partial \ln V)_T$	Volume dependence of Grüneisen parameter	–
X_i	Mole fraction of the i-th melt component	–
σ_i	Effective sphere diameter	m
$\overline{V}_m$	Volume occupied by a mole of molecules	m^3 mol^{-1}
$f = \overline{V}_m/\overline{V}$	Packing fraction	–
y_1, y_2	Interactions among different spheres	–
$\Phi = P\overline{V}/RT$	Dimensionless compressibility factor	–
μ	Exponent of the attractive term in EOS	–
ν	Exponent of the repulsive term in EOS	–
$\eta_i = (\partial \ln \sigma_i/\partial \ln T)_{\overline{V}}$	Temperature dependence of sphere diameter	–
$\xi_i = 3(\partial \ln \sigma_i/\partial \ln \overline{V})_T$	Volume dependence of sphere diameter	–
$\vartheta_i = (\partial \ln \overline{V}_{m0i}/\partial T)_{\overline{V}}$	Temperature dependence of $\overline{V}_{m0i}$	K^{-1}
$\omega = (\partial \xi/\partial T)_{\overline{V}}$	Temperature dependence of ξ	K^{-1}
$\zeta = (\partial \xi/\partial \ln \overline{V})_T$	Volume dependence of ξ	–
$\tau = d\xi/df$	Dependence of ξ on packing fraction	–
$\theta = (\partial \ln \overline{V}_m/\partial T)_{\overline{V}}$	Temperature dependence of the volume of spheres	K^{-1}
$c_{Na_2O–Al_2O_3}$	Cross composition term	–

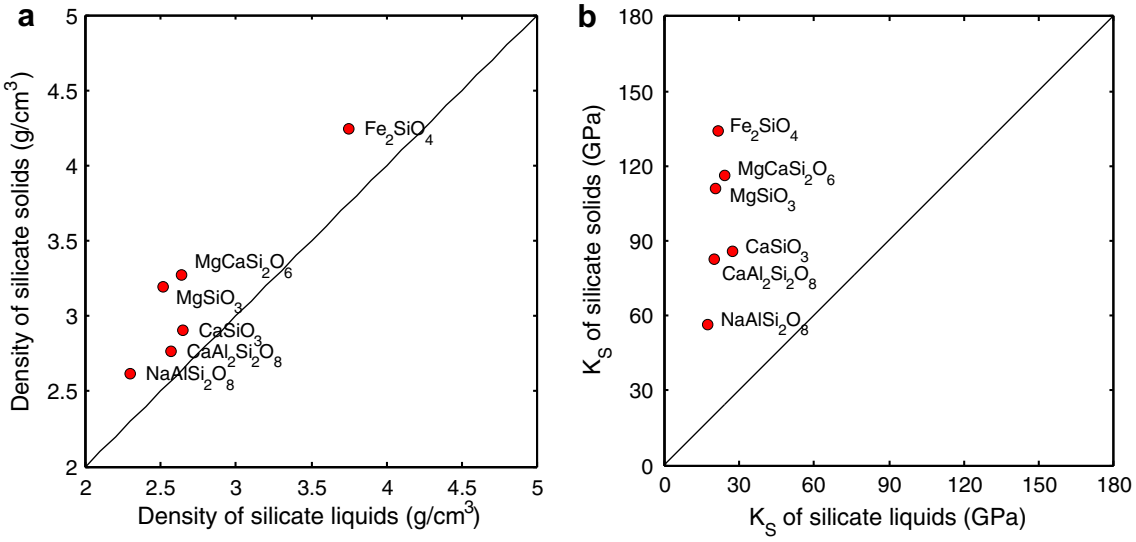

Fig. 1. Comparison of room-pressure compressional properties for some silicate liquids and solids. (a) Density; (b) bulk modulus. Experimental data are from the compilation of Bass (1995). Diagonal lines show 1:1 correlation between the axes.

solids for these silicates fall on the same lines on this plot, which implies that glasses have the same compression mechanism as crystals. On the contrary, liquids are significantly more compressible than solids and glasses compared at the same molar volume. This implies that the differences in bulk modulus between liquids and solids (and glasses) cannot be attributed to the differences in molar volume (mean interatomic distance) only: the entropy contribution to compression must be important for liquids.

2.2. The pressure dependence of Grüneisen parameter

Another important difference in compressional properties between liquids and solids is the volume (pressure) dependence of Grüneisen parameter. The Grüneisen parameter (γ) and its volume dependence (q) are defined as (Anderson, 1995)

$$\gamma = \frac{\alpha K_T V}{C_V} \tag{3}$$

and

$$q = \left(\frac{\partial \ln \gamma}{\partial \ln V}\right)_T. \tag{4}$$

It has been demonstrated by first-principles molecular dynamics (FPMD) studies (Stixrude and Karki, 2005; Karki et al., 2006, 2007; de Koker et al., 2008; Stixrude et al., 2009) that the Grüneisen parameters of liquids including $MgSiO_3$, Mg_2SiO_4, SiO_2, and MgO increase with increasing compression (q in Eq. (4) is negative) as opposed to solids for which the Grüneisen parameters decrease upon compression (Anderson, 1995). This observation has also been supported by shock-wave studies on silicate liquids (Mosenfelder et al., 2009; Asimow and Ahrens, 2010). Other non-metallic liquids including water and some organic liquids also have the negative volume dependence ($q < 0$) (Boehler and Kennedy, 1977; Brown et al., 1988).

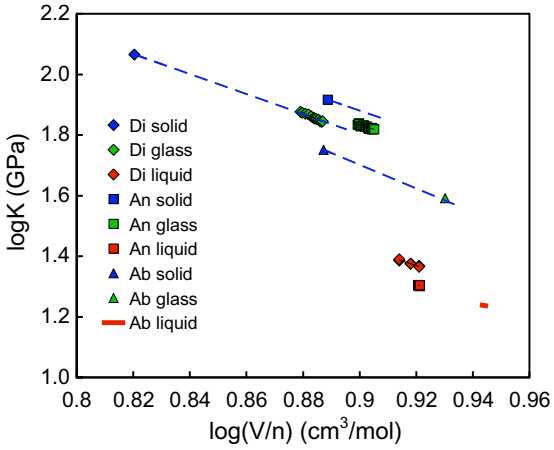

Fig. 2. Bulk modulus–molar volume relationships for silicate crystals, glasses, and liquids. Data for crystals, glasses, and liquids are shown in blue, green, and red, respectively. Diamonds, squares, and triangles are for Di, An, and Ab, respectively. Blue dashed lines are predictions of Birch's law, which are calculated based on the temperature derivative of bulk modulus and thermal expansion for Di, and the pressure derivatives of bulk modulus for An and Ab. The bulk modulus and molar volume data are from Ai and Lange (2008) for liquid Di and An, Kress et al. (1988) for liquid Ab, Schilling et al. (2003) for glassy Di and An, and Wang (1989) for glassy Ab. The bulk modulus of solid Di and its temperature derivative are from Isaak et al. (2006). The bulk modulus of solid An and Ab are from Angel (2004) and Tenner et al. (2007), respectively. The molar volume and thermal expansivity of solid Di at room-pressure are from Levien et al. (1979) and Fei (1995), respectively. Molar volume of solid An and Ab at ambient conditions are from Smyth and McCormick (1995) and Tenner et al. (2007), respectively. The pressure derivative of bulk modulus for An and Ab are from Angel (2004) and Tenner et al. (2007), respectively. (For interpretation of the references to color in this figure legend, the reader is referred to the web version of this article.)

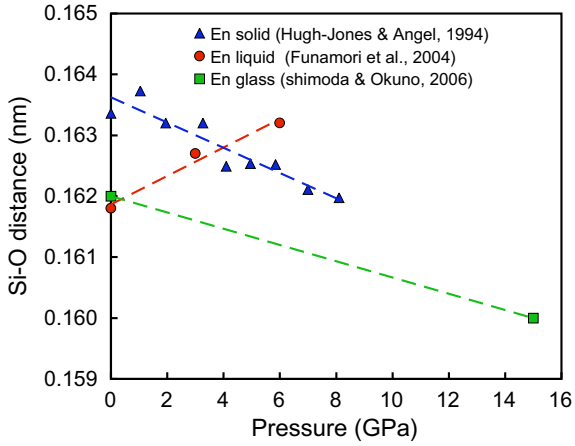

Fig. 3. Si–O interatomic distances in the $MgSiO_3$ solid, glass, and liquid at elevated pressures. The results for the liquid and the glass are from Funamori et al. (2004) and Shimoda and Okuno (2006), respectively. The average Si–O bond distance for orthoenstatite is calculated from the results on the unit cell parameters at high pressure by Hugh-Jones and Angel (1994).

2.3. Radial distribution functions

The different behaviors of liquids, glasses, and solids upon compression are also suggested by the studies on the structural change with increasing pressure. The bond length in liquids (average distance of the nearest neighbor atoms) can be obtained by studying the radial distribution function of liquids (RDF) using X-ray scattering (e.g., Funamori et al., 2004; Yamada et al., 2007) or molecular dynamics (MD) simulations (e.g., Karki et al., 2007). Fig. 3 shows the change in the Si–O bond distance as a function of pressure for the $MgSiO_3$ solid (in the orthoenstatite phase), glass and liquid. It can be seen that the Si–O bond distance increases with pressure in the $MgSiO_3$ liquid, while it decreases in the $MgSiO_3$ crystal and glass with similar pressure dependencies. This is consistent with other observations that the compression mechanisms of liquids are different from solids and glasses and implicates that much of the compression in silicate liquids occurs through the geometrical arrangement of liquid building blocks whose sizes do not change much with compression, i.e., the entropic mechanism of compression plays a dominant role over the internal energy contribution. These differences in compressional properties between liquids and solids cannot be fully understood by previous EOS models in the geological literature, which are based on either the purely empirical approaches or based on the physical models developed for solids.

3. FORMULATION OF THE EQUATION OF STATE

3.1. Basic concepts of the hard sphere model for liquids

The interatomic potential may be separated into the short-range repulsive part and the long-range attractive part (see textbooks on theories of liquids, e.g., Hansen and McDonald, 2006). Molecular dynamics simulations on liquids have shown that the repulsive part of the potential controls the structure (or geometrical arrangement) of the liquids (Chandler, 1978). The repulsive potential can be further simplified as the hard sphere potential, where the molecules in the liquids are considered as rigid spheres (with infinite strength) and they can move freely as far as they do not overlap. The mutual interaction of molecules is included only by the excluded volume effect (i.e., influence of finite size of spheres). The pressure in the hard sphere model is caused entirely by the entropy and the EOS of a liquid takes a form that resembles that of a gas, viz.,

$$P = \frac{RT}{\overline{V}}\Phi(f), \tag{5}$$

where $\overline{V}$ is the molar volume of the liquid, R is the gas constant, and $\Phi(f)$ is a function that represents the excluded volume effect with f being the packing fraction defined as

$$f \equiv \frac{\overline{V}_m}{\overline{V}}, \tag{6}$$

where $\overline{V}_m$ is the volume occupied by a mole of spheres. For a monatomic liquid, $\overline{V}_m$ is given by

$$\overline{V}_m = \frac{1}{6}\pi\sigma^3 N_A, \tag{7}$$

where σ is the diameter of hard spheres; N_A is the Avogadro's constant. By taking the volume derivative of Eq. (5), and using $(\partial f/\partial \overline{V})_T = -f/\overline{V}$, one can obtain the bulk modulus of the hard sphere liquids as

$$K_T = \frac{RT}{\overline{V}}\Gamma(f) = \frac{RT}{\overline{V}}\frac{d}{df}[f\Phi(f)]. \tag{8}$$

The key is to formulate $\Phi(f)$ in Eqs. (5) and (8) for various physical models of liquids.

For the one-component system, the equation of state of hard sphere liquids can be given as (Reiss et al., 1959; Thiele, 1963; Wertheim, 1963),

$$\Phi(f) = \frac{1 + f + f^2}{(1-f)^3}, \tag{9}$$

and hence

$$\Gamma(f) = \frac{1 + 4f + 4f^2}{(1-f)^4}. \tag{10}$$

Eq. (9) successfully explains the results from numerical simulations on hard sphere liquids (e.g., Henderson, 1964).

Guillot and Sarda (2006) first applied the hard sphere EOS to the compression of some silicate melts assuming the melt is a single component system. Although the effect of composition cannot be studied by the one-component hard-sphere EOS, the success of Guillot and Sarda (2006) shows its potential as a starting point for a more precise EOS for silicate liquids. To illustrate this, here we show that the hard sphere EOS naturally explains the compressional properties of silicate liquids reviewed in Section 2.

First, as seen from Eq. (8) the bulk modulus of a hard sphere liquid depends strongly on the packing fraction of the liquid, which is a result of the entropy-dominated compression (through the excluded volume effect). Upon compression, the bulk modulus increases as the packing

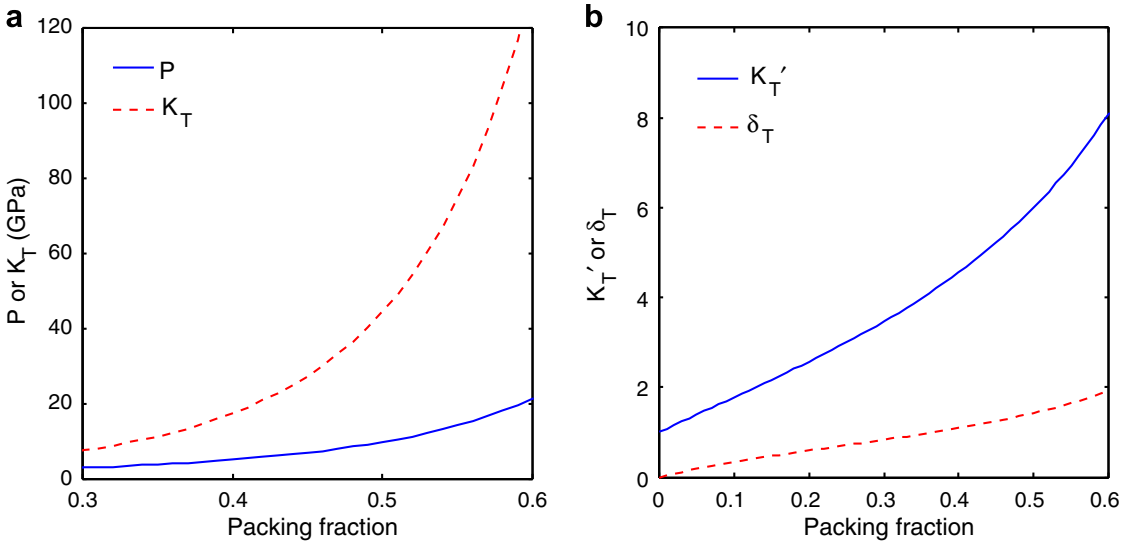

Fig. 4. Results of the simple hard sphere equation of state for a liquid with a molar volume of 20 cm^3/mol at 1673 K. (a) P and K_T as functions of packing fraction. (b) K_T' and δ_T as functions of packing fraction.

fraction increases (Fig. 4a). Guillot and Sarda (2006) discovered that for a wide range of melt compositions including silica, MORB, peridotite, komatiite, and olivine melts, the reduced density ρ^* (defined as $N_A\sigma^3/\overline{V}$) "is remarkably constant" ($\rho^* = 0.803 \pm 0.025$). Therefore the packing fraction (Eqs. (6) and (7)) takes a narrow range of $\sim 0.42 \pm 0.01$ at room pressure. This corresponds to a narrow range of bulk modulus that is consistent with the observation (Fig. 1b).

Second, the hard sphere model predicts a volume (pressure) dependence of Grüneisen parameter that is consistent with the observations for non-metallic liquids. To demonstrate this, we calculate the volume dependence of Grüneisen parameter (Eq. (3)) using the volume dependencies of thermal expansivity, bulk modulus, and heat capacity. The volume dependence of heat capacity has not been measured experimentally for silicate liquids, but was estimated to be relatively small and negligible using thermodynamic relations (Bottinga, 1985). Results of first-principles molecular dynamic simulations on silicate liquids (e.g., Stixrude and Karki, 2005; Karki et al., 2006, 2007; de Koker et al., 2008) showed the change in heat capacity over the pressure range of 130 GPa is about 10%. From thermodynamic relations, the volume dependencies of thermal expansivity and bulk modulus can be defined as non-dimensional parameters

$$\delta_T = \left(\frac{\partial \ln \alpha}{\partial \ln V}\right)_T \tag{11}$$

and

$$K_T' = -\left(\frac{\partial \ln K_T}{\partial \ln V}\right)_T. \tag{12}$$

For the simple hard sphere EOS, α can be obtained by taking the temperature derivative of Eq. (5) as

$$\alpha = \frac{1}{K_T}\left(\frac{\partial P}{\partial T}\right)_V = \frac{1}{T}\frac{(1-f)(1+f+f^2)}{1+4f+4f^2}. \tag{13}$$

Then K_T' and δ_T can be obtained by taking the volume derivatives of Eqs. (8) and (13)

$$K_T' = \frac{1+9f+2f^2}{1+f-2f^2} \tag{14}$$

$$\delta_T = \frac{f(4+3f^2+2f^3)}{(1-f^3)(1+2f)}. \tag{15}$$

Fig. 4b shows the calculated K_T' and δ_T as functions of f for the simple hard sphere liquid. The Grüneisen parameter as a function of volume is therefore given by

$$\gamma = \gamma_0\left(\frac{\overline{V}_0}{\overline{V}}\right)^{-q}, \tag{16}$$

with

$$q = \delta_T - K_T' + 1. \tag{17}$$

From thermodynamic relations

$$K_T' - \delta_T = \frac{1}{\alpha K_T}\left(\frac{\partial K_T}{\partial T}\right)_V \tag{18}$$

is the intrinsic temperature dependence of bulk modulus. This quantity controls the behavior of γ upon compression. For materials following the Birch's law, $K_T' = \delta_T$ (Anderson, 1989) and $q = 1$, which is consistent with observations (e.g., Anderson, 1974; Boehler and Ramakrishnan, 1980; Stixrude and Lithgow-Bertelloni, 2005). For hard sphere liquids, from Eqs. (14) and (15), we have

$$K_T' - \delta_T = \frac{(1+2f)^2}{1-f^3}. \tag{19}$$

Therefore for a packing fraction (f) larger than 0, $K_T' - \delta_T > 1$, and $q < 0$ for hard sphere liquids, which means that the Grüneisen parameter increases with increasing pressure.

These predictions agree qualitatively with the observations summarized in Section 2. However, the hard sphere model cannot make quantitative predictions to actual silicate liquids given the complex interatomic interactions

that differ from the hard sphere potential. In the following, we will make some modifications to the hard sphere model in two different but closely related aspects. First, when we treat actual silicate liquids with complex compositions, we need to extend this equation of state to a multi-component system. Second, in the simplest form, the hard sphere EOS involves only the entropy term. Changes in internal energy will certainly occur in a realistic liquid. This effect needs to be included in the actual application of this type of equation of state to silicate melts under deep Earth conditions.

3.2. Equation of state for hard sphere mixtures

We adopt the equation of state for a hard sphere mixture generalized from Eq. (9) by solving the Percus–Yevick equation (Lebowitz, 1964; Lebowitz et al., 1965) to account for the multiple components in silicate liquids such as SiO_2 and MgO. It should be noted that similar equations with higher accuracy have been developed for the hard sphere mixtures (Mansoori et al., 1971; Hansen-Goos and Roth, 2006), but we use the Percus–Yevick equation as a starting point for its simplicity. For a liquid composed of neutrally charged hard spheres of different sizes (i.e., no interaction between the hard spheres except for the excluded volume effect), $\Phi(f)$ becomes

$$\Phi(f,y_1,y_2)=\frac{1+(1-3y_1)f+(1-3y_2)f^2}{(1-f)^3}, \tag{20}$$

where

$$f=\frac{\overline{V}_m}{\overline{V}}=\sum_{i=1}^{m} f_i, \tag{21}$$

m is the number of components in the liquid and

$$\overline{V}_m=\sum_{i=1}^{m} X_i\overline{V}_{mi}=\frac{1}{6}\pi N_A\sum_{i=1}^{m} X_i\sigma_i^3 \tag{22}$$

$$f_i=\frac{\overline{V}_{mi}X_i}{\overline{V}}=\frac{1}{6\overline{V}}\pi\sigma_i^3X_iN_A, \tag{23}$$

where σ_i and X_i are the hard sphere diameter and the mole fraction of the i-th component. X_i is normalized as $\sum_{i=1}^{m}X_i=1$. y_1 and y_2 are the parameters representing the interaction of spheres with different sizes. They are functions of σ_i and X_i, and are independent of molar volume.

$$y_1=\sum_{j>i=1}^{m}\Delta_{ij}(\sigma_i+\sigma_j)(\sigma_i\sigma_j)^{-1/2}, \tag{24}$$

$$y_2=\sum_{j>i=1}^{m}\Delta_{ij}\sum_{k=1}^{m}\left(\frac{f_k}{f}\right)\frac{(\sigma_i\sigma_j)^{1/2}}{\sigma_k}, \tag{25}$$

with

$$\Delta_{ij}=[(f_if_j)^{1/2}/f][(\sigma_i-\sigma_j)^2/\sigma_i\sigma_j](X_iX_j)^{1/2}. \tag{26}$$

Again, the bulk modulus can be obtained by taking the volume derivative of the equation of state (Ashcroft and Langreth, 1967; Tomczyk, 1977; Suski and Tomczyk, 1981)

$$\Gamma(f,y_1,y_2)=\frac{\partial}{\partial f}(f\Phi)=\frac{1+(4-6y_1)f+(4-3y_1-9y_2)f^2}{(1-f)^4}. \tag{27}$$

3.3. Attractive force and the internal energy contribution

The hard sphere mixture model developed for neutrally charged spheres cannot be applied to real liquids directly because there is no attractive force and the zero-pressure volume is infinite (see Eqs. (5) and (20)). Since we will use room-pressure data to place constraints on sphere sizes, it is necessary to introduce the attractive interaction. The attraction in silicate liquids comes mainly from the Coulombic interactions between cations (such as Mg^{2+} and Si^{4+}) and anions (O^{2-}) in the liquids. The straightforward approach is to develop a theory for charged hard sphere mixtures. Despite the vast literature on this subject, available analytical models are mostly limited to the simplest case: the restricted primitive model for binary mixtures with equally sized and charged ions (Blum et al., 1992; Fisher and Levin, 1993; Zhou and Stell, 1995; Zhou et al., 1995; Guillot and Guissani, 1996), which is far less complicated than real silicate liquid.

Since our purpose is to develop a simple equation of state of silicate liquids that can be readily used for geochemical and geophysical modeling, we choose a more empirical approach by modifying the hard sphere EOS with a mean-field adjustment. Longuet-Higgins and Widom (1964) showed that for simple molecular liquids, the structure of liquids is mostly determined by the steeply changing repulsive potential, which can be approximated as the hard sphere potential, whereas the slowly varying attractive potential can be introduced as a uniform negative background potential. This mean field approach was later extended to ionic liquids by Itami and Shimoji (1980) and McBroom and McQuarrie (1983). Following this approach, we consider a silicate liquid as a mixture of hard spheres corresponding to different melt components such as SiO_2 and MgO, and consider the electrostatic energy as a uniformly distributed negative background potential, which does not change the structure of a liquid but will modify the thermodynamic properties of liquids. Then the cohesion energy can be viewed as a liquid analog of the Madelung energy of solids. The equation of state is given as

$$P=\frac{RT}{\overline{V}}\Phi(f,y_1,y_2)-\frac{A}{\overline{V}^{\mu}}, \tag{28}$$

where μ is an exponent that depends on the nature of the attractive force and is 4/3 for the Coulombic attraction and A is a constant of volume that describes the importance of the internal energy contribution. A can be evaluated by setting $P=0$ in Eq. (28).

$$A=RT\Phi_0\overline{V}_0^{\mu-1}, \tag{29}$$

where $\Phi_0=\Phi(f_0,y_{10},y_{20})$ and subscript "0" represents room pressure values. Substituting (29) back into (28), one gets

$$P=\frac{RT}{\overline{V}}\left[\Phi-\Phi_0\left(\frac{\overline{V}_0}{\overline{V}}\right)^{\mu-1}\right]. \tag{30}$$

The isothermal bulk modulus can then be obtained as

$$K_T=\frac{RT}{\overline{V}}\left[\Gamma-\mu\Phi_0\left(\frac{\overline{V}_0}{\overline{V}}\right)^{\mu-1}\right], \tag{31}$$

where Φ and Γ are given in Eqs. (20) and (27). At $P = 0$, the room-pressure bulk modulus is

$$K_{T0} = \frac{RT}{\overline{V}_0}[\Gamma_0 - \mu\Phi_0]. \quad (32)$$

4. APPLICATION OF THE EQUATION OF STATE TO SILICATE LIQUIDS

We consider a 5-component system including SiO_2, Al_2O_3, FeO, MgO, and CaO (hereafter referred to as the CMASF system) as an example to demonstrate how the proposed EOS is applied to real silicate liquids.

4.1. Application of the equation of state to room-pressure data

In this section, we calibrate the proposed EOS using room-pressure data on density (or molar volume) and bulk modulus. The proposed EOS (Eq. (30)) has a few parameters including the room-pressure molar volume $\overline{V}_0$ and the volume occupied by a mole of the hard spheres $\overline{V}_m$. Both $\overline{V}_0$ and $\overline{V}_m$ are compositional dependent. $\overline{V}_0$ also depends on temperature. $\overline{V}_m$ is calculated from the hard sphere diameters (σ_i) (Eq. (22)).

The room-pressure molar volume ($\overline{V}_0$) is well described by the ideal mixing model (e.g., Bottinga and Weill, 1970; Lange, 1997), viz.,

Table 2
Sources of room-pressure relaxed sound velocity data.

System	Sample	Number of observations	Temperature (K)
Ai and Lange (2008)			
SiO_2–Al_2O_3–CaO	RC-14	6	1837–1880
	LC-4	6	1780–1884
	LC-8	5	1809–1883
SiO_2–Al_2O_3–MgO–CaO	LC-9	5	1790–1893
	LC-10	6	1727–1873
	LC-11	8	1746–1895
	LC-12	6	1736–1893
	LC-13	8	1758–1887
	SN-4	2	1817–1881
SiO_2–MgO–CaO	SN-13	6	1736–1893
	LC-14	6	1699–1887
	LC-15	10	1683–1893
Webb and Courtial (1996)			
SiO_2–Al_2O_3–CaO	Ca53.12	36	1623–1823
	Ca38.27	27	1673–1823
Secco et al. (1991)			
SiO_2–Al_2O_3–MgO–CaO	$An_{36}Di_{64}$	2	1558–1831
Rivers and Carmichael (1987)			
SiO_2–MgO–CaO	Di	6	1698–1758
SiO_2–Al_2O_3–CaO	An	4	1833
SiO_2–CaO	$CaSiO_3$	4	1836
SiO_2–Al_2O_3–MgO–CaO	$An_{50}Di_{50}$	8	1573–1673
SiO_2–FeO	Fe_2SiO_4	2	1503–1653
	Fs-2	7	1598–1693
SiO_2–Na_2O	$Na_2Si_2O_5$	8	1556–1693
	Na_2SiO_3	2	1458–1573
SiO_2–K_2O	$K_2Si_2O_5$	2	1553–1693
SiO_2–MgO	$MgSiO_3$	4	1913
SiO_2–Al_2O_3–MgO–CaO–Na_2O	$Ab_{50}Di_{50}$	6	1598–1698
	$Ab_{33}An_{33}Di_{33}$	3	1698
SiO_2–MgO–Na_2O	SN-10	2	1663–1723
SiO_2–Al_2O_3–FeO–MgO–CaO–Na_2O	Jor-44	6	1703–1803
Kress et al. (1988)			
SiO_2–Al_2O_3–Na_2O	8	6	1599–1684
	9	7	1594–1695
	10	5	1891
	15	2	1690
	B	5	1891
	K	13	1689–1894
SiO_2–Na_2O	A (1–11)	11	1487–1683
	A (12–20)	7	1556–1693

$$\overline{V}_0 = \sum_{i=1}^{m} \overline{V}_{0i} X_i. \quad (33)$$

Note that the mole fraction defined in this study is different from the common definition used in the ideal mixing model, since a mole of Al_2O_3 has two moles of Al^{3+} cations and hence will be considered as two moles of spheres. As a result, the molar volume for $AlO_{1.5}$, which is half of the molar volume of Al_2O_3, must be applied in Eq. (33). The ideal mixing model is widely used and can give excellent results on melt densities (within 1% to experimental values). Therefore the same approach is applied here to calibrate $\overline{V}_0$. The hard sphere diameter (σ_i) for each melt component is then calibrated by room-pressure bulk modulus using Eq. (32). The room-pressure bulk modulus can be obtained by ultrasonic sound velocity measurements

$$\frac{1}{K_{T0}} = \frac{\overline{V}_0}{c^2} + \frac{T\overline{V}_0\alpha_0^2}{C_{P0}}, \quad (34)$$

where c is the measured sound velocity for silicate liquids. α_0 and C_{P0} are room-pressure values of the thermal expansivity and heat capacity of silicate liquids, which can be calculated by the ideal-mixing model (e.g., Lange and Navrotsky, 1992; Lange, 1997).

For the CMASF system, we start from the most recent data set on sound velocity given by Ai and Lange (2008) to calibrate our equation of state. In addition to this data set, results of Webb and Courtial (1996), Secco et al. (1991), and Rivers and Carmichael (1987) are also included in the calibration. Only relaxed sound velocity data that do not depend on the frequency of the measurements are used. The sources of the experimental data used in the calibration are summarized in Table 2. Excluding the data for FeO-bearing liquids, this data set is similar to the one used in Ai and Lange (2008) to calibrate the ideal-mixing model of compressibility for CMAS liquid. In total, 170 observations are included in the data set for 21 different compositions. Room-pressure molar volume and thermal expansivity are calculated from the ideal-mixing model. Partial molar quantities except for the FeO component are from the calibration of Lange (1997). For the FeO component, results of Kress and Carmichael (1991) are used. Room-pressure heat capacity C_{P0} is calculated from the calibration of Lange and Navrotsky (1992).

A non-linear least squares regression with five parameters in total for the 5-component system was conducted. Regressed results of σ_i for each cation are listed in Table 3 along with the one-sigma error (σ) estimates for the parameters. Fig. 5 shows the comparison of the predicted

Table 3
Calibrated hard-sphere diameters for melt components in the CMASF system using Eq. (32).

Component	σ_i (nm)
SiO_2	0.3346 ± 0.0006
Al_2O_3	0.3001 ± 0.0004
FeO	0.2761 ± 0.0007
MgO	0.2628 ± 0.0012
CaO	0.3099 ± 0.0007

Uncertainties represent one σ error estimates. The adjusted R^2 for the regression is 0.848. The root mean squared error (s) of the fit is 0.589.

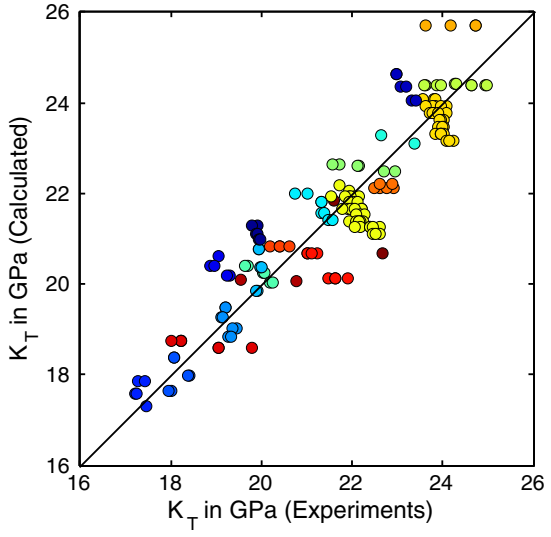

Fig. 5. Comparison of the predicted room-pressure bulk modulus K_{T0} for the CMASF system using the proposed EOS and parameters in Table 3 with experimental data. Symbols with different colors represent different melt compositions. Symbols with the same color are for the same melt composition but measured at different temperatures and frequencies. The diagonal line shows 1:1 correlation of the axes. (For interpretation of the references to color in this figure legend, the reader is referred to the web version of this article.)

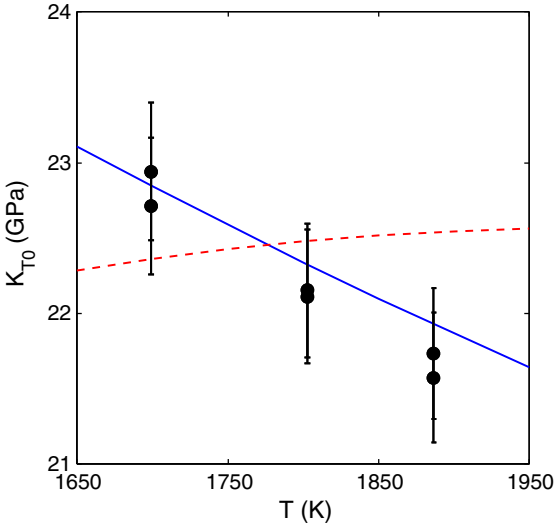

Fig. 6. Comparison of the predicted room-pressure bulk modulus for $CaMgSi_2O_6$ (Di) liquid with experimental results. The red dashed curve is the calculated K_{T0} using temperature-independent sphere diameters in Table 3; the blue solid curve is the calculated K_{T0} using temperature-dependent sphere diameters in Table 4; The black solid circles are the experimental results of Ai and Lange (2008). (For interpretation of the references to color in this figure legend, the reader is referred to the web version of this article.)

K_{T0} and experimental measurements for the different melt compositions represented by different colors. The overall goodness of the fit is fair with a maximum residual in K_{T0} of about 2 GPa (10%). The adjusted R^2 is 0.848 and the root mean squared error (s) of the fit is 0.589. A detailed analysis of Fig. 5 reveals that with one parameter for each melt component, the proposed model can explain the effect of composition fairly well. However, the predicted results for each composition at various temperatures are less satisfactory. For example, Fig. 6 shows that the predicted K_{T0} for the diopside (Di) melt increases with increasing temperature (dashed line), which is opposite to the temperature dependence of experimental data (solid circles) from Ai and Lange (2008). This comparison indicates that the model with constant sphere sizes can explain properties such as the compositional dependence but must be modified in order to explain the temperature dependence of bulk modulus.

4.2. Temperature dependence of sphere diameters

We introduce the temperature dependence of hard sphere diameters by considering the fact that the repulsive potential between two spheres in the liquids is not precisely the hard sphere potential, i.e., spheres have finite strength. As a result, the potential energy is higher but remains finite when the distance between spheres is smaller. At a higher temperature, the kinetic energy is higher due to the higher average velocity of the spheres. The kinetic energy can be converted to the potential energy of spheres during the elastic collision of spheres, and as a result the effective sphere diameters decrease with increasing temperature (e.g., Stillinger, 1961; Andersen et al., 1971). For the inverse power law repulsive potential that was widely used for soft spheres (e.g., Rowlinson, 1964; Ben-Amotz and Stell, 2004), the effective sphere diameter (σ) can be evaluated by equating the repulsive potential energy to the kinetic energy at temperature T

$$\frac{\varepsilon}{\sigma^s} = k_B T. \tag{35}$$

where ε is a constant, s is the power of the potential. Therefore the effective hard-sphere diameter for the i-th component is

$$\sigma_i(T) = \sigma_{i,T_{ref}} \left(\frac{T_{ref}}{T}\right)^{\frac{1}{s_i}}, \tag{36}$$

where $\sigma_{i,T_{ref}}$ is the hard sphere diameter at the reference temperature T_{ref}. Therefore we can define the temperature dependence of σ_i as

$$\eta_i \equiv \frac{d\ln\sigma_i}{d\ln T} = -\frac{1}{s_i}. \tag{37}$$

Using the same set of experimental data for the CMASF system in Table 2, we conduct another non-linear least squares regression to constrain $\sigma_{i,T_{ref}}$ and η_i (10 parameters in total for the 5-component system, which is identical to the number of parameters used in the ideal-mixing model when calculating room-pressure bulk modulus). Calibrated $\sigma_{i,T_{ref}}$ and η_i with one-sigma error estimates for each component are listed in Table 4. The relative uncertainties in the fitted hard sphere diameters are rather small (~0.1–0.3%). However, the uncertainties in the temperature dependence of hard sphere diameter are large because the temperature range in sound velocity measurements (see Table 2) is not very large (less than 250 K, and only 100 K for many compositions). It should also be noted that η_i is positive for the MgO component, which is inconsistent with our physical picture of the temperature effect on hard-sphere diameters. This may be either due to the complex interaction between different melt components (for example, the Mg–O coordination likely depends on temperature and melt composition (George and Stebbins, 1998)), or due to the narrow temperature range of the sound velocity data, which will be better constrained when experimental data for a larger temperature range become available.

Table 4
Calibrated hard-sphere diameters and their temperature dependencies for melt components in the CMASF system using Eq. (32).

Component	$\sigma_{i,T_{ref}}$ (nm)	$\eta_i = d\ln\sigma_i/d\ln T$
SiO_2	0.3356 ± 0.0004	-0.08 ± 0.01
Al_2O_3	0.3012 ± 0.0003	-0.04 ± 0.01
FeO	0.2744 ± 0.0004	-0.01 ± 0.02
MgO	0.2627 ± 0.0007	0.14 ± 0.04
CaO	0.3102 ± 0.0006	-0.02 ± 0.02

Reference temperature (T_{ref}) is 1673 K. Uncertainties represent one σ error estimates. The adjusted R^2 for the regression is 0.981. The root mean squared error (s) of the fit is 0.073.

The predicted bulk moduli for CMAS liquids using the parameters in Table 4 are compared with experimental

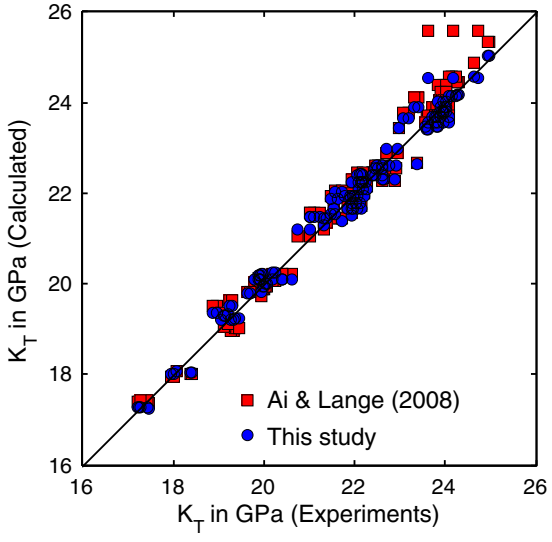

Fig. 7. Comparison of the predicted room-pressure bulk modulus K_{T0} for the CMASF system with experimental measurements. Blue circles represent the predictions of the proposed EOS and parameters in Table 4; red squares represent the predictions of Ai and Lange (2008). (For interpretation of the references to color in this figure legend, the reader is referred to the web version of this article.)

results in Fig. 7. The overall fit has been significantly improved from the previous regression (Fig. 5). The adjusted R^2 is 0.981 and the root mean squared error (s) of the fit is 0.073. We also compare our results with those of the ideal-mixing model by Ai and Lange (2008) in Fig. 7 as similar data sets were used for the calibration of both models. The predictions made by the proposed EOS are as good as the ideal-mixing model. The solid line in Fig. 6 shows that the calculated room-pressure bulk modulus for $CaMgSi_2O_6$ (Di) liquid as a function of temperature is consistent with the experimental observations from Ai and Lange (2008). Thus the proposed equation of state with temperature-dependent sphere diameters can reproduce the room-pressure bulk modulus and its temperature dependence well at least for the Di composition (but not limited to the Di composition as suggested by the improved fitting in Fig. 7 from Fig. 5).

Table 5
Calibrated hard-sphere diameters and their temperature dependencies for melt components in the CMASFNK system using Eq. (32).

Component	$\sigma_{i,T_{ref}}$ (nm)	$\eta_i = d\ln\sigma_i/d\ln T$
SiO_2	0.3371 ± 0.0005	-0.06 ± 0.02
Al_2O_3	0.3031 ± 0.0006	-0.12 ± 0.03
FeO	0.2730 ± 0.0008	-0.04 ± 0.04
MgO	0.2610 ± 0.0013	0.08 ± 0.06
CaO	0.3065 ± 0.0009	0.01 ± 0.03
Na_2O	0.3517 ± 0.0010	0.12 ± 0.03
K_2O	0.4007 ± 0.0037	0.17 ± 0.15

Reference temperature (T_{ref}) is 1673 K. Uncertainties represent one σ error estimates. The adjusted R^2 for the regression is 0.963. The root mean squared error (s) of the fit is 0.431.

4.3. Calibrations for liquids with more components

Using the same approach demonstrated for the CMASF system, we also calibrate our proposed EOS for liquids with seven components including CaO, MgO, FeO, Al_2O_3, SiO_2, Na_2O, and K_2O (CMASFNK). Again, the room-pressure molar volume, thermal expansion, and heat capacity are calculated from the ideal-mixing model as for the CMASF system. In addition to the sound velocity data for the CMASF system, experimental data from Kress et al. (1988) and Rivers and Carmichael (1987) on Na- and K-bearing melts are included in the calibration (Table 2). There is only one composition that contains K_2O in the data set. Results on K_2SiO_3 from Rivers and Carmichael (1987) are excluded since the sample dissolved a significant amount of MoO_2 (4.7 wt%) in the melt. Some other ultrasonic results on the potassium-bearing liquids including Bockris and Kojonen (1960) and Baidov and Kunin (1968) are not included in the regression since the measured sound velocities cannot be confirmed to be relaxed (Lange and Carmichael, 1990; Kress and Carmichael, 1991). In total, there are 259 observations of sound velocity data for 37 different liquid compositions.

The calibrated hard sphere diameters and their temperature dependencies for the 7-component system are listed in Table 5. The uncertainties in the parameters for the K_2O component are quite large compared to other components due to the limited number of samples that contain K_2O. Fig. 8a shows the comparison of model predicted bulk moduli with experimental values. The overall fitting is good with an adjusted R^2 of 0.963 and s of 0.431. For most compositions without Na_2O, the residuals are less than 1 GPa (better than 5%). However, for the Na-bearing liquids, the predicted results are less good with a maximum

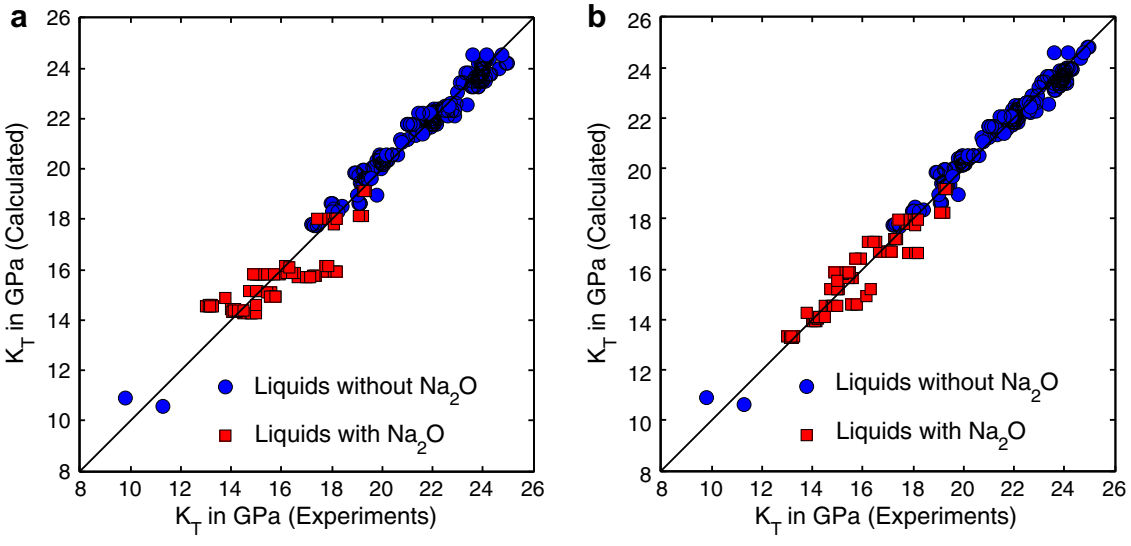

Fig. 8. Comparison of the predicted room-pressure bulk modulus K_{T0} for the CMASFNK system using the proposed EOS with experimental data. Red squares represent Na_2O-bearing liquids and blue circles represent Na_2O-free compositions. (a) Regression results without the interaction term between Na_2O and Al_2O_3 (regressed parameters are in Table 5); (b) regression with the interaction term between Na_2O and Al_2O_3 (regressed parameters are in Table 6). (For interpretation of the references to color in this figure legend, the reader is referred to the web version of this article.)

Table 6
Calibrated hard-sphere diameters and their temperature dependencies for melt components in the CMASFNK system using Eq. (32) with the Na_2O–Al_2O_3 interaction term (Eq. (38)).

Component	$\sigma_{i,T_{ref}}$ (nm)	$\eta_i = d\ln\sigma_i/d\ln T$
SiO_2	0.3370 ± 0.0004	-0.06 ± 0.01
Al_2O_3	0.3010 ± 0.0004	-0.05 ± 0.02
FeO	0.2732 ± 0.0006	-0.04 ± 0.03
MgO	0.2607 ± 0.0010	0.10 ± 0.04
CaO	0.3084 ± 0.0007	-0.05 ± 0.02
Na_2O	0.3466 ± 0.0008	-0.04 ± 0.03
K_2O	0.4010 ± 0.0026	0.16 ± 0.11
$c_{Na_2O-Al_2O_3}$	0.17 ± 0.01[a]	–

Reference temperature (T_{ref}) is 1673 K. Uncertainties represent one σ error estimates. The adjusted R^2 for the regression is 0.981. The root mean squared error (s) of the fit is 0.221.
[a] $c_{Na_2O-Al_2O_3}$ is a non-dimensional parameter.

residual of 2.3 GPa (~15%). This is possibly due to the interaction between the Na_2O and the Al_2O_3 components to maintain local charge balance, which has already been reported by Kress et al. (1988) and Ghiorso and Kress (2004) for the ideal mixing model of bulk modulus. In these models, better fitting results were achieved by introducing the Na_2O–Al_2O_3 cross-composition term, i.e., a composition dependent partial molar compressibility for the Na_2O component.

Similarly, cross-composition terms can also be introduced to the proposed EOS by assuming compositional dependent hard sphere diameters. In the case of Na_2O–Al_2O_3 interaction, the effective hard sphere diameter for the Na_2O component can be given by including an interaction parameter $c_{Na_2O-Al_2O_3}$

$$\sigma'_{Na_2O} = \sigma_{Na_2O}(1 + X_{Al_2O_3} c_{Na_2O-Al_2O_3}). \quad (38)$$

It is likely that K_2O interacts with Al_2O_3 too, but a K_2O–Al_2O_3 interaction term cannot be resolved due to the scarce data on K_2O-bearing melts. Therefore in this study, only Na_2O–Al_2O_3 interaction term is included. Calibrated parameters with the Na_2O–Al_2O_3 cross term are listed in Table 6, and compared with measurements in Fig. 8b. It can be seen that most parameters except for the results of the Na_2O and Al_2O_3 components remain similar values as the previous regression (Table 5) and the regression for the CMASF system (Table 4), while the hard-sphere diameter for the Na_2O component increases with the Al_2O_3 component. The introduction of the interaction term significantly improves the overall fitting with an adjusted R^2 of 0.981 and s of 0.221.

4.4. Prediction of density at high pressure and the deformability of spheres

If the assumption that spheres have infinite strength remains valid at high pressure, then we can apply the EOS for high-pressure properties without introducing additional parameters. Given the calibrated EOS parameters for the CMASF system in Table 4 as well as the room pressure molar volumes calculated from the ideal-mixing model, we calculate the compressional curves for a few peridotitic melts (Fig. 9a) and basaltic melts (Fig. 9b) whose densities were measured by the sink/float experiments (Agee and Walker, 1993; Suzuki et al., 1998; Suzuki and Ohtani, 2003). It can be seen that the predicted densities of all melt compositions are somewhat smaller than the experimental data especially at high pressures. The assumption of constant sphere size at high pressure has to be modified in order to explain the density data at high pressure.

A straightforward modification is to introduce the volume dependence of the sphere diameters. For the i-th component,

$$\sigma_i(T) = \sigma_{i0}(T)\left(\frac{\overline{V}}{\overline{V}_0}\right)^{\frac{\xi_i}{3}}, \quad (39)$$

where ξ_i defines the deformability of the i-th sphere and is assumed to be independent of $\overline{V}$ and T for simplicity. The volume of molecules changes upon compression can be defined as a deformability parameter, viz.,

$$\xi \equiv \left(\frac{\partial \ln \overline{V}_m}{\partial \ln \overline{V}}\right)_T = \frac{1}{\overline{V}_m}\sum_{i=1}^{m} X_i \overline{V}_{mi}\xi_i. \quad (40)$$

The volume derivatives of all other quantities that depend on $\overline{V}_m$ should also be modified accordingly using Eq. (40). For example, the volume dependence of packing fraction changes to

$$\frac{\partial f}{\partial \overline{V}} = \frac{f}{\overline{V}}(\xi - 1). \quad (41)$$

Similarly, the equation of state should be different than Eq. (28) since it is obtained by taking the volume derivative of Helmholtz free energy of the liquids. The entropic contribution (excluded volume effect) to the Helmholtz free energy has the form of (e.g., Hansen and McDonald, 2006)

$$F_{ev} = RT\left[\ln\frac{f}{1-f} + \frac{3}{2}\frac{(2f - f^2)}{(1-f)^2}\right]. \quad (42)$$

Taking the volume derivative of Eq. (42) gives

$$P_{ev} = \frac{RT}{\overline{V}}(1-\xi)\Phi, \quad (43)$$

which is different from Eq. (5) by a factor of $(1-\xi)$ due to the deformability of the spheres. The attractive energy term (Coulombic term) remains the same as in Eq. (28) since it is a long-range interaction and does not depend on $\overline{V}_m$.

In addition to the entropic contribution and the attractive energy term, the repulsive energy also needs to be considered to account for the strain energy stored in the deformed spheres. We assume the repulsive potential takes the same inverse power-law form for all melt components, that is, $U_{rep} \propto 1/\sigma_m^s \propto 1/\overline{V}_m^{v-1}$, where $v = s/3 + 1$. Note that the repulsive energy is a short-range potential, which controls the local structure of a liquid and hence should be a function of $\overline{V}_m$. Based on the results of ionic crystals, s can be related to K'_{T0} of the material (e.g., Poirier, 2000) as $K'_{T0} = (s+7)/3$. If K'_{T0} is 4 as in the case of many crystals, then s has a value of about 5. The pressure due to the repulsive energy can be given by

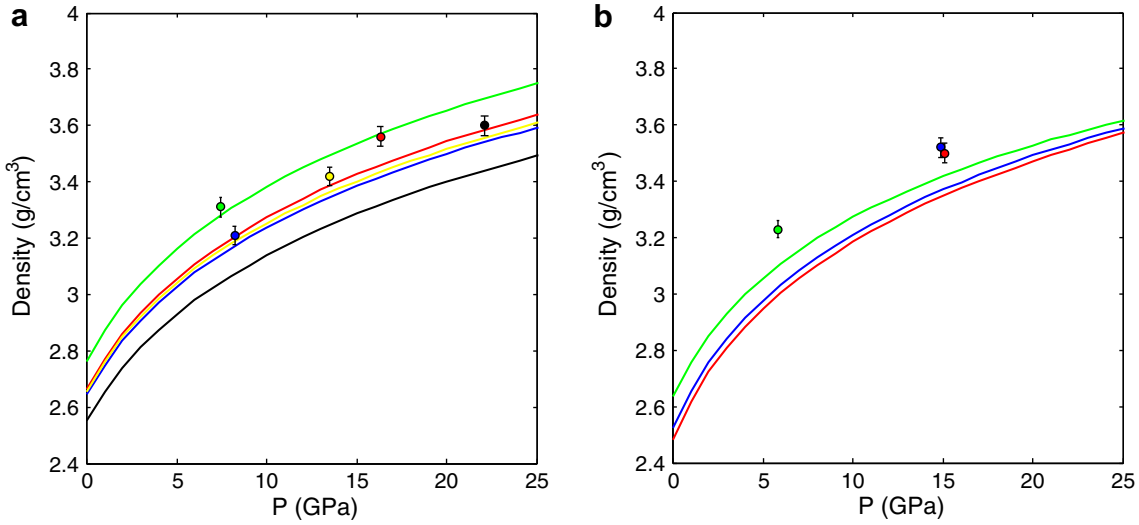

Fig. 9. Compression curves calculated from the proposed equation of state assuming spheres are rigid at high pressures. Parameters in Table 4 are used. (a) Peridotitic melts; (b) basaltic melts. Different colors represent different melt compositions. Experimental results (symbols) were determined by the sink/float technique (see Table 7 for data sources). (For interpretation of the references to color in this figure legend, the reader is referred to the web version of this article.)

$$P_{rep} = -\frac{\partial U_{rep}}{\partial \overline{V}} \propto (v-1) f \xi \frac{1}{\overline{V}_m^v}. \tag{44}$$

Combining Eqs. (43), (44), and (28), we obtain the modified equation of state considering the deformability of spheres

$$P = \frac{RT}{\overline{V}}(1-\xi)\Phi - \frac{A}{\overline{V}^{\mu}} + \frac{f\xi B}{\overline{V}_m^v}, \tag{45}$$

where $\mu = 4/3$ and $v = 8/3$; A and B are constants that do not depend on volume. B can be obtained by letting $\xi = 1$ and $P = 0$. Eq. (45) then reduces to

$$B = \frac{\overline{V}_{m0}^{v-1}}{\overline{V}_0^{\mu-1}} A. \tag{46}$$

Constant A can be obtained by letting $\xi = 0$ and $P = 0$. The result for A is the same as in Eq. (29). Substituting Eq. (29) and (46) back to Eq. (45), the final form of the equation of state can be derived as

$$P = \frac{RT}{\overline{V}}\left[(1-\xi)\Phi - \Phi_0\left(\frac{\overline{V}_0}{\overline{V}}\right)^{\mu-1} + \xi\Phi_0\left(\frac{\overline{V}_{m0}}{\overline{V}_m}\right)^{v-1}\right], \tag{47}$$

and the bulk modulus can be obtained by taking the volume derivative of Eq. (47)

$$K_T = \frac{RT}{\overline{V}}\left[(1-\xi)^2\Gamma + (\zeta + (1-\xi)\xi)\Phi - \mu\Phi_0\left(\frac{\overline{V}_0}{\overline{V}}\right)^{\mu-1} + \Phi_0(\xi - \zeta + (v-1)\xi^2)\left(\frac{\overline{V}_{m0}}{\overline{V}_m}\right)^{v-1}\right], \tag{48}$$

where

$$\zeta = \frac{\partial \xi}{\partial \ln \overline{V}} = \frac{1}{\overline{V}_m}\sum_{i=1}^{m} X_i \overline{V}_{mi}\xi_i^2 - \xi^2. \tag{49}$$

The room-pressure bulk modulus is thus given by

$$K_{T0} = \frac{RT}{\overline{V}_0}\left[(1-\xi_0)^2\Gamma_0 + \Phi_0(2\xi_0 + (v-2)\xi_0^2 - \mu)\right]. \tag{50}$$

Table 7
Sources of high-pressure density data from sink/float experiments.

Composition	Sample	Pressure (GPa)	Temperature (K)	Sources
Peridotitic	KLB-1	8.2	2273	Agee and Walker (1993)
	IT8720	16.3	2543	Suzuki et al. (1998)
	MA	16	2603	Suzuki et al. (1998)
	MA	7.4	2163	Suzuki et al. (1998)
	PHN1611	13.5	2303	Suzuki and Ohtani (2003)
	PHN1611	20.5	2633	Suzuki and Ohtani (2003)
	Pyrolite	22.1	2633	Suzuki and Ohtani (2003)
Picritic	Picrite	14.5	2773	Ohtani and Maeda (2001)
Komatiitic	Komatiite	8.9	2173	Agee and Walker (1993)
	Komatiite	6	2073	Agee and Walker (1993)
Basaltic	MORB	5.85	1673	Agee (1998)
	MORB	14.9	2473	Ohtani and Maeda (2001)
	MORB	15.1	2773	Ohtani and Maeda (2001)

Table 8
Calibrated sphere diameters and their temperature dependencies for melt components in the CMASF system assuming the sphere diameters are also volume dependent.

Component	$\sigma_{i,T_{ref}}$ (nm)	$\eta_i = (\partial \ln \sigma_i / \partial \ln T)_{\overline{V}}$	$\xi_i = 3(\partial \ln \sigma_i / \partial \ln \overline{V})_T$
SiO_2	0.365 ± 0.001	-0.02 ± 0.01	0.62 ± 0.04
Al_2O_3	0.328 ± 0.002	-0.03 ± 0.01	0.66 ± 0.06
FeO	0.257 ± 0.008	0.00 ± 0.02	-0.68 ± 0.28
MgO	0.277 ± 0.002	0.00 ± 0.02	0.22 ± 0.07
CaO	0.335 ± 0.003	-0.14 ± 0.02	0.66 ± 0.08

Reference temperature (T_{ref}) is 1673 K. Uncertainties represent one σ error estimates.

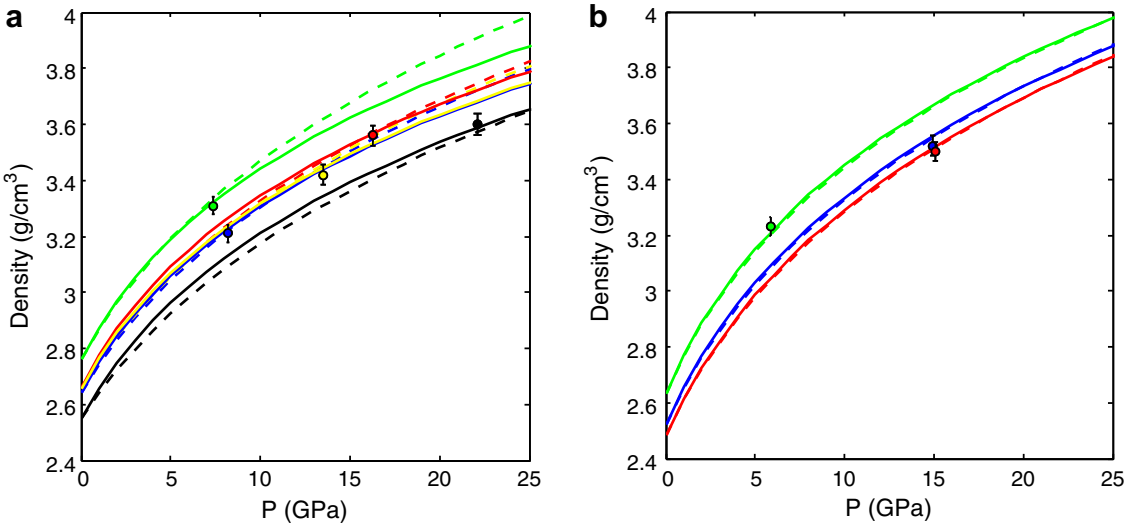

Fig. 10. Compression curves calculated from the proposed equation of state assuming that spheres are deformable at high pressure. (a) Peridotitic melts; (b) basaltic melts. Different colors represent different melt compositions. Experimental results (symbols) were determined by the sink/float technique (see Table 7 for data sources). Solid lines are calculated by assuming component-specific volume dependencies of sphere diameters (ξ_i), using parameters in Table 8. Dashed lines are calculated by assuming a single ξ for all components, using parameters in Table 9. (For interpretation of the references to color in this figure legend, the reader is referred to the web version of this article.)

Table 9
Calibrated sphere diameters and their temperature dependencies for melt components in the CMASF system assuming the sphere diameters are also volume dependent.

Component	$\sigma_{i,T_{ref}}$ (nm)	$\eta_i = (\partial \ln \sigma_i / \partial \ln T)_{\overline{V}}$	$\xi = 3(\partial \ln \sigma / \partial \ln \overline{V})_T$
SiO_2	0.3612 ± 0.0006	-0.03 ± 0.01	0.53 ± 0.01[a]
Al_2O_3	0.3242 ± 0.0006	-0.02 ± 0.01	
FeO	0.2935 ± 0.0007	-0.02 ± 0.02	
MgO	0.2827 ± 0.0007	0.08 ± 0.01	
CaO	0.3311 ± 0.0008	-0.12 ± 0.02	

Reference temperature (T_{ref}) is 1673 K. Uncertainties represent one σ error estimates.
[a] ξ takes the same value for all melt components.

The deformability of spheres (ξ_i) must be constrained by high-pressure experimental data. Table 7 summarizes the density data determined from sink/float experiments. A regression was conducted using Eqs. (47) and (50) simultaneously with data in Tables 2 and 7 by minimizing $[\sum_i (P_i - P)^2 + \sum_j (K_{T0j} - K)^2]$, where P_i is the pressure for the i-th density measurement and K_{T0j} is the bulk modulus for the j-th bulk modulus measurement. The regressed parameters are listed in Table 8. Predicted compression curves are plotted as solid lines in Fig. 10a for peridotitic melts and in Fig. 10b for basaltic melts. In contrast to Fig. 9a and b, the density data at high pressure can be reproduced very well. The residuals in calculated density and experimental measurements are less than 1% and about

0.5% for most compositions, which are similar to the experimental uncertainties. Therefore the introduction of the deformability of spheres can significantly improve the fitting for high-pressure density data.

Since the regressed values of ξ_i have large uncertainties due to the limited data at high pressures, we may simplify the model by using an average ξ in the regression. Using the same data sets (Tables 2 and 7), we can obtain the EOS parameters in Table 9. Predicted compression curves based on this model are shown as dashed lines in Fig. 10a and b. It can be seen that the density data can be reproduced quite well by using a single $\xi = 0.53$ for all component, although there exists some difference between the predicted compression curves.

4.5. Predictions of other compressional properties at high pressure

In this section we use a Fe-rich peridotitic melt composition MA (see Suzuki et al. (1998) for the chemical composition of this melt) as an example to demonstrate how the proposed equation of state can be applied to calculate compressional properties at high pressure including bulk modulus (K_T), thermal expansivity (α), and Grüneisen parameter (γ). Bulk modulus (K_T) can be calculated directly from Eq. (48). Fig. 11a shows the calculated K_T as a function of pressure for the MA melt at 2603 K. The pressure derivative of bulk modulus (K'_{T0}) is estimated to be about 7.0. Thermal expansivity (α) as a function of pressure can be obtained by taking the temperature derivative of Eq. (47). The detail derivation of thermal expansivity at high pressure is presented in Appendix B. Fig. 11b shows that thermal expansivity for the MA melt decreases from about $1 \times 10^{-4}\,K^{-1}$ at room pressure to about $5.4 \times 10^{-5}\,K^{-1}$ at 25 GPa. From Eq. (11), The volume dependence of thermal expansivity (δ_T) can be estimated to be about 2.1, which is much smaller than the typical values for solids (about 4).

Given the calculated results for bulk modulus (K_T), and thermal expansivity (α) at high pressure, Grüneisen parameter (γ) can be calculated using Eq. (3). Fig. 11c shows that the predicted Grüneisen parameters for the MA melt decreases with compression. The volume dependence of Grüneisen parameter (q) can be estimated (from its definition in Eq. (4)) to be about -3.9, which is a negative value in contrast to $q = 1$ for materials that follow Birch's law. According to Eq. (17), the negative value of q for liquids comes mainly from the distinct thermal properties of liquids represented by a small value of δ_T compared to K'_T, which is a direct consequence of the entropy contribution as

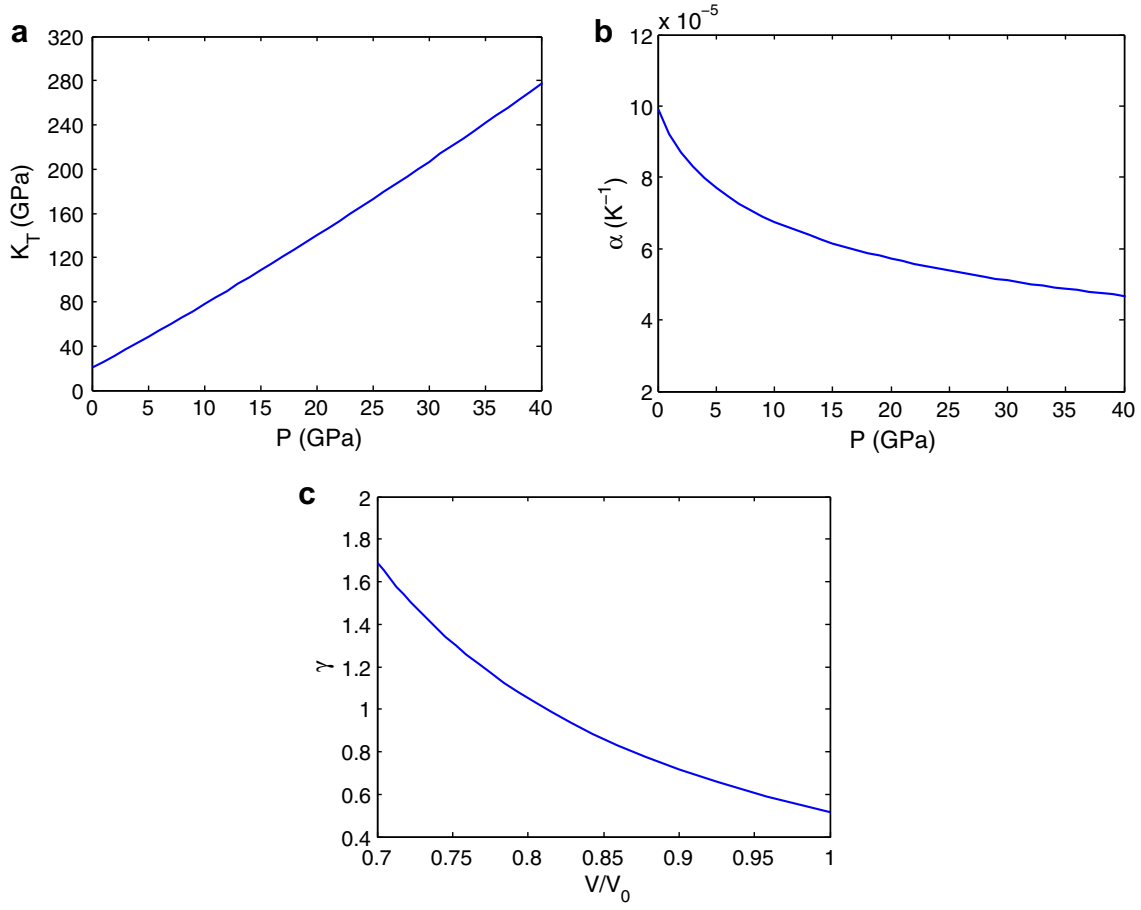

Fig. 11. Predicted compressional properties at high pressures for the peridotitic melt MA at 2603 K. (a) Bulk modulus; (b) thermal expansivity; (c) Grüneisen parameter.

demonstrated by the simple hard-sphere model. If we compare the predicted volume dependence of Grüneisen parameter (q) with previous results on silicate liquids, we find that the calculated value is somewhat smaller (larger in absolute value) than the estimates (about −1.6 to −2.0) from numerical simulations and shock-wave experiments on the Mg_2SiO_4 and $MgSiO_3$ liquids (Stixrude and Karki, 2005; Mosenfelder et al., 2009). Two factors may contribute to this discrepancy: basically the influence of compression and temperature. (1) The prediction of the Grüneisen parameter for the MA melt is based on the calibration of EOS using experimental data up to only 25 GPa, but the observations are based on shock-wave experiments and numerical simulations that cover a much larger range of pressure from room pressure to 130 GPa. The extrapolation of the EOS to such high pressures will introduce some uncertainty in the calculated Grüneisen parameter due to the uncertainties in the calibrated sphere diameters and their volume dependencies. (2) The calculated volume dependence of Grüneisen parameter (q) is obtained for an isothermal compression at 2603 K, but both shock-wave data and numerical simulation results were obtained at very high temperatures from 3000 to 6000 K or even higher and q was assumed to be a constant of temperature in these studies. That is, the previous estimated q is an average value over a wide range of high temperatures. We will discuss the application of our EOS to these very high pressure–temperature conditions in the next section.

4.6. Application of the EOS to extreme pressures up to 130 GPa

Our previous calibration of the EOS parameters (Tables 8 and 9) is limited to sink/float data up to 25 GPa. The

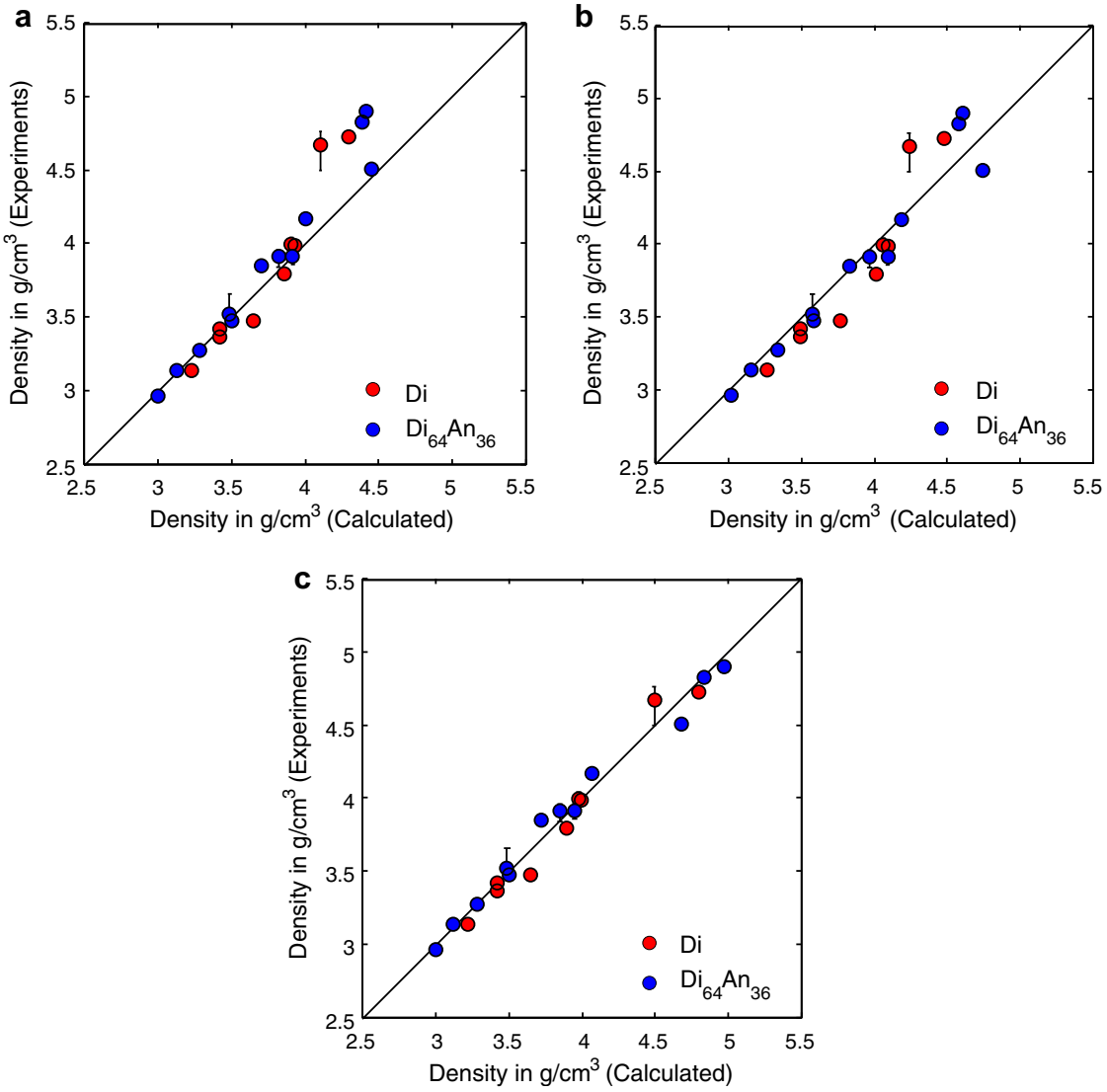

Fig. 12. Comparison of predicted density for Di (blue circles) and Di_{64}–An_{36} (red circles) with shock-wave data. (a) EOS parameters in Table 9 are used; (b) shock data are included in the calculation; (c) the deformability of spheres is assumed to depend on the packing fraction of the liquid. Parameters in Table 11 are used. The diagonal line shows 1:1 correlation of the axes. (For interpretation of the references to color in this figure legend, the reader is referred to the web version of this article.)

validity of this calibration at very high pressures may be examined by the density data determined by shock-wave experiments from 5 to 130 GPa (e.g., Rigden et al., 1988, 1989; Miller et al., 1991; Chen et al., 2002; Asimow and Ahrens, 2010). Fig. 12a compares the calculated density for Di (diopside) and $Di_{64}An_{36}$ (diopside–anorthite eutectic) using the proposed EOS and parameters in Table 9 to the density determined by shock-wave experiments (Asimow and Ahrens, 2010). The shock temperatures for the data are calculated based on the P–V–T EOS provided in Asimow and Ahrens (2010) (Table 10). The difference between the predicted density and experimental data is less than 1% at 40 GPa, but increases with pressure and can be as large as 10% at pressures higher than 80 GPa. Consequently, the previous calibration may not be applicable to pressures higher than 40 GPa.

Ideally, we can incorporate all shock-wave data into our data set to extend the pressure range of the EOS. However, most shock data currently available have poorly estimated shock temperatures due to two major reasons: (1) The volume dependence of the Grüneisen parameter (q) is often assumed to be 1 in these calculations, which is not consistent with the new observations for liquids (e.g., Asimow and Ahrens, 2010); (2) The specific heat (C_V) is often assumed to be 3R/mol atm (the Dulong–Petite value for solid materials), which could be more than 50% less than the real liquid values (Richet and Neuville, 1992). The combination of these two can result in an uncertainty in shock temperature of more than 1000 K, which is a serious problem for the EOS calibration given the large thermal expansivity of silicate melts at high pressure. Therefore we will only include the shock data for Di and $Di_{64}An_{36}$ melts from Asimow and Ahrens (2010) to calibrate our EOS since the Grüneisen parameter and its volume dependence (q) were better determined from their data without just assuming $q = 1$. Anorthite (An) melt has also been studied in Asimow and Ahrens (2010) but will not be included in the calibration because the data show some very complicated compressional behavior (a possible abrupt structural change at high pressure), which may require two equations of state for both pressure ranges below and above the transition pressure.

Table 10
Estimated shock temperatures for Di and $Di_{64}An_{36}$ based on the shock data and EOS provided in Asimow and Ahrens (2010).

Composition	Pressure (GPa)	Density (g/cm^3)	Shock temperature (K)
Di	8.7	3.14	1861
	13.9	3.36	1999
	14.1	3.42	2048
	21.5	3.47	2093
	32.8	3.79	2496
	38.2	4	2908
	39.3	3.99	2885
	84.7	4.67	5562
	114.3	4.73	5943
$Di_{64}An_{36}$	4.5	2.96	1765
	6.7	3.14	1836
	10	3.27	1902
	15.6	3.52	2081
	15.8	3.47	2038
	24.2	3.85	2473
	29.3	3.91	2572
	33.8	3.91	2572
	41.3	4.17	3139
	85.8	4.51	4426
	109.9	4.83	6822
	127.5	4.9	7647

Since shock data for only two compositions will be included in the calculation, the deformability of spheres (ξ_i) for each melt component will be difficult to resolve at high pressure. Consequently, we will use a single deformability parameter (ξ) for all components for the calibration. In addition, the shock temperatures are higher when the pressures are higher, which makes the volume dependence of sphere diameters hard to be isolated from the temperature dependence. To avoid this trade-off between the temperature and volume dependencies, we use the same temperature dependence of sphere diameters in Table 9 calibrated by using ultrasonic data and sink/float data. After including the shock data for Di and Di_{64}–An_{36} (Table 10), the new regression gives a higher deformability ($\xi = 0.63$) compared to the previous value of 0.53. Fig. 12b compares the predicted density with that determined by shock experiments. Although the calculation of the density at pressures higher than 80 GPa is improved, the calculated melt densities are too high at relatively low pressures due to the high deformability of spheres. This means the predicted melts are too compressible at relatively low pressures but not compressible enough at high pressures. A likely reason for this is that the deformability of spheres may not be constant but depend on the packing fraction of the liquid when the EOS is applied over a wide range of pressures such as from room pressure to 130 GPa.

A simple way to model this behavior is to define the deformability of spheres to be a linear function of the packing fraction as

$$\xi \equiv \left(\frac{\partial \ln \overline{V}_m}{\partial \ln \overline{V}}\right)_T = \xi_0 + \tau(f - f_0), \tag{51}$$

where ξ_0 is the deformability of spheres at room pressure and τ determines how packing fraction influences ξ. The equation of state remains the same as Eqs. (47), (48), and (50), but it should be noted that $\zeta = (\partial\xi/\partial \ln \overline{V})_T$ in Eq. (48) becomes

$$\zeta = -\tau f(1 - \xi). \tag{52}$$

To solve the EOS, f and $\overline{V}_m$ can be expressed as functions of $\overline{V}$. Using Eq. (51), it can be shown that

$$\frac{d \ln \overline{V}}{d \ln f} = \frac{1}{(\xi_0 - 1) + \tau(f - f_0)}. \tag{53}$$

Then $\overline{V}$ can be integrated out as a function of f. After some manipulation, one obtains

$$f = f_0 \frac{\tau f_0 + (1 - \xi_0)}{\tau f_0 + (1 - \xi_0)(\overline{V}/\overline{V}_0)^{\tau f_0 + (1 - \xi_0)}}. \tag{54}$$

Then the volume of spheres at high pressure can be obtain from

$$\overline{V}_m = f\overline{V}. \tag{55}$$

Table 11
Calibrated sphere diameters and their temperature and volume dependencies for melt components in the CMASF system assuming that the deformability of spheres depends on packing fraction.

Component	$\sigma_{i,T_{ref}}$ (nm)	$\eta_i = (\partial \ln \sigma_i / \partial \ln T)_{\overline{V}}$	ξ_0	τ
SiO_2	0.350 ± 0.002	-0.03 ± 0.01[a]	0.31 ± 0.03[b]	0.84 ± 0.05[b]
Al_2O_3	0.315 ± 0.001	-0.02 ± 0.01[a]		
FeO	0.287 ± 0.001	-0.02 ± 0.02[a]		
MgO	0.279 ± 0.001	0.08 ± 0.01[a]		
CaO	0.325 ± 0.001	-0.12 ± 0.02[a]		

Reference temperature (T_{ref}) is 1673 K. Uncertainties represent one σ error estimates.
[a] Same values of η_i in Table 9 are used.
[b] All melt components have the same values of ξ_0 and τ.

Again, we use Eqs. (47) and (50) to calibrate all the data including sound velocity data (Table 2), sink/float density data (Table 7), and the shock-wave density data (Table 10). The regressed ξ_0 and τ are 0.31 and 0.84, respectively (Table 11). Given that the packing fractions for Di and Di_{64}–An_{36} change from about 0.4–0.5 at room pressure to about 0.65–0.75 at 130 GPa, the deformability of spheres increases from 0.31 to about 0.5. Fig. 12c shows the comparison of the predicted density with experimental data. The experimental data can be reproduced well and no systematic deviation is observed in this case. Consequently, with a packing-fraction dependent deformability, the proposed EOS can be successfully applied to model density data at extreme pressures up to 130 GPa.

Now we can calculate the Grüneisen parameter at extreme pressures up to 130 GPa Eq. (3). The formulation to calculate the thermal expansivity (α) is given in Appendix B. The calculated Grüneisen parameters for the peridotitic melt MA at high pressures and various temperatures from 2000 to 6000 K are plotted in Fig. 13 and compared with observations. It can be seen that the volume dependence of Grüneisen parameter (q) increases with temperature from about −3 at 2000 K to about −2 at 4000 K and to about −1 at 6000 K. The predicted q at 4000 K are consistent with the observations that were averaged over 3000–6000 K. A likely explanation for the temperature effect on q is that with increasing temperature the packing fraction is smaller due to small sphere diameters and as we have demonstrated in Fig. 4b for the simple hard sphere liquid, the difference between the pressure derivative of bulk modulus (K'_T) and volume dependence of thermal expansivity (δ_T) is smaller at lower packing fraction. That is, q increases with decreasing packing fraction (the absolute value of q decreases) and eventually becomes 0 for the ideal gas.

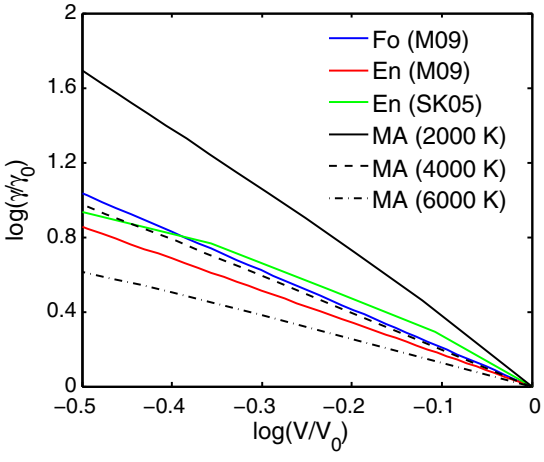

Fig. 13. Grüneisen parameters as functions of compression for a peridotitic melt (MA) at 2000, 4000, and 6000 K. Also shown are the results for forsterite (Fo) and enstatite (En) from shock-wave experiments (M09, Mosenfelder et al. (2009)) and numerical simulations (SK05, Stixrude and Karki (2005)).

5. DISCUSSION

5.1. Interpretation of the sphere diameters

The hard sphere (deformable sphere actually) picture is a simplification of the very complex structure of silicate melts, which varies dramatically depending on the melt composition and pressure (e.g., McMillan and Wolf, 1994; Stebbins, 1995; Wolf and McMillan, 1995; Mysen and Richet, 2005, and references therein). This means that the sphere diameters cannot be measured directly and cannot provide the complete structural information of melts. It is however interesting to compare the inferred sphere diameters from our model with the bond lengths in crystalline solids (Fig. 14). It can be seen that for the components with 6-fold coordination including FeO, MgO, CaO, Na_2O, and K_2O, there is a correlation between the calibrated sphere diameters and bond lengths in the crystals. This correlation suggests that the short-range order for the 6-fold species is correctly represented by the proposed model. For the components with the 4-fold coordination including SiO_2 and Al_2O_3, however, they do not follow the high-coordination trend. The possible explanation is that the geometry of the effective volume (excluded volume) occupied by species with 4-fold coordination deviates considerably from a sphere, essentially due to the strong directional covalent bonding in these species. Therefore a large empty space is included if we treat the excluded volumes of these species as spheres. This implies that if the coordination of these species (SiO_2, Al_2O_3) changes to 6-fold, the influence of the directed covalent bonding will become weak and the sphere volumes of these species will become smaller. Thus this provides a possible explanation for the high deformability of spheres for SiO_2 and Al_2O_3 compared to MgO: the deformability parameter (ξ_i) is 0.62 for SiO_2 and 0.66 for Al_2O_3, but only 0.22 for MgO (Table 8). With increasing pressure, SiO_2 and Al_2O_3 can undergo a gradual

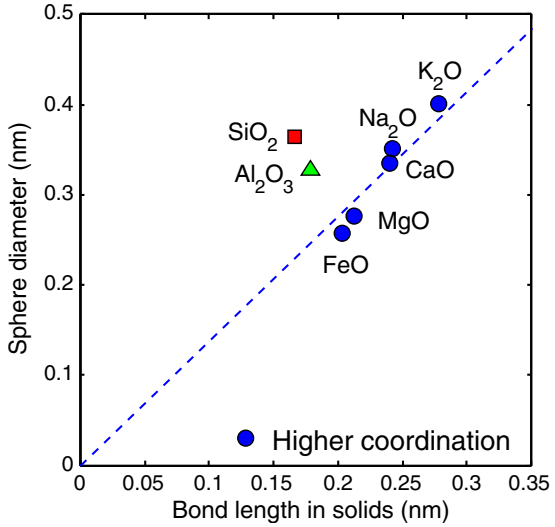

Fig. 14. Comparison of effective sphere diameters for melt components with the bond lengths in crystals at room pressure. The dashed line shows the correlation between the sphere diameters and bond lengths for components with higher coordination than 4.

coordination change from 4-fold to 6-fold, as demonstrated by both experiments and numerical simulations (e.g., Xue et al., 1989; Wolf and McMillan, 1995; Lee et al., 2004; Stixrude and Karki, 2005). During the coordination change, most of the empty space in the 4-fold species becomes available to oxygen atoms and as a result the sphere diameters become much smaller. The small deformability of MgO, on the other hand, may be explained by the change in the Mg–O bond length (soft interatomic potential) or the small difference between the 6- and 8-fold coordination.

5.2. Limitations of the model and future developments

We recommend the EOS parameters listed in Table 8 be used to calculate compressional properties of silicate melts when pressure is lower than 40 GPa. Fifteen parameters in total are calibrated for the CMASF system based on room-pressure bulk modulus data and high-pressure density data up 25 GPa from sink/float experiments. The bulk modulus data focus mainly on SiO_2–Al_2O_3–MgO–CaO melts: only two compositions include FeO. The temperature range in these measurements is within 300 K, which limits the calibration of the temperature dependence of sphere diameters. On the other hand, most melts in sink/float experiments are ultramafic to mafic composition. Therefore the use of the proposed EOS for very MgO poor melts at high pressures may produce larger uncertainties. In addition, there is a trade-off between the sphere diameter and its temperature and volume dependencies. More density measurements and maybe sound velocity measurements at high pressures for wide ranges of temperature and melt compositions are required to better constrain the EOS parameters.

For pressures higher than 40 GPa, we recommend the parameters listed in Table 11 be used. In total 12 parameters are used in this calibration. The packing-fraction dependence of deformability becomes more important at extreme pressures. Density data including shock-wave data and first-principles molecular dynamics calculations at extreme pressure and temperature conditions are critical to constrain the EOS behavior under such conditions. It is possible that the functional forms for the temperature and volume dependencies of sphere diameters may need further modifications with more data become available. In that case, the first-principles molecular dynamics calculations, which are helpful to find the link between microscopic properties and the model parameters, may provide some insights and guidelines for such modifications.

At the current stage, we have not considered the effect of oxidation state of the FeO component. Fe_2O_3 is expected to have very different properties than FeO (e.g., Kress and Carmichael, 1991). Volatile components such H_2O, and CO_2 are also very important to the density of silicate liquids (Lange, 1994).

We have made simple empirical approximations for the cohesion energy and the soft repulsive potential of hard spheres. This means that the structure of liquids is not explicitly modeled in the EOS, but represented by the sphere parameters and their temperature and volume dependencies. As a result, the sphere diameters cannot be measured directly and the exact structural information cannot be derived from the equation of state. For example, the effect of increasing coordination for the network modifiers such as SiO_2 and Al_2O_3 with increasing compression may contribute to the deformability of those spheres as we discussed in the previous section, but the exact coordination of these species cannot be calculated. Polymerization is another complication introduced by the network-forming components like SiO_2 and Al_2O_3, which can be linked to other network-forming components through bridging oxygen to form a chain-like or a three-dimensional network of molecules (for the review of polymerization refer to Mysen and Richet, 2005, and the references therein). Polymerization may reduce the entropy of the liquids and in turn affect the other properties such as compressibility and viscosity. If this effect is important, compositional dependent sphere diameters may be needed to model the network-forming components. However, since most data on density and bulk modulus can be explained well by the proposed EOS, the effect of polymerization on the entropic contribution to compression (excluded volume of spheres) is likely small. This on the other hand means that the proposed model cannot be applied to study the liquid structure and structure-related properties such as transport properties without introducing more parameters for the structural information.

ACKNOWLEDGMENTS

This work was supported by the National Science Foundation. Constructive reviews by Dave Yuen, two anonymous reviewers and Associate Editor Bjorn Mysen have significantly improved the manuscript.

APPENDIX A. BULK MODULUS–MOLAR VOLUME RELATIONSHIP FOR SOLIDS AND BIRCH'S LAW

Birch's law is an empirical relationship between elastic constants (wave velocities) and density proposed by Birch (1961). Its physical interpretations and implications have been discussed in detail in many works (e.g., Birch, 1961; Anderson and Nafe, 1965; Chung, 1972; Shankland, 1972). Here we summarize the main conclusions below.

For solids, the free energy is mainly from the interatomic potential energy. Therefore the bulk modulus of solids is controlled by the molar volume or mean interatomic distance. For a given material, the volume derivatives of bulk modulus at constant temperature or constant pressure are given by

$$\left(\frac{\partial \ln K_T}{\partial \ln V}\right)_T = -K'_T \tag{A1}$$

and

$$\left(\frac{\partial \ln K_T}{\partial \ln V}\right)_P = -\delta_T, \tag{A2}$$

where K'_T is the pressure derivative of bulk modulus and δ_T is the Anderson–Grüneisen parameter. If we define mean atomic weight as $\overline{M}_a = \overline{M}/n$, where $\overline{M}$ is the molar formula weight and n is the number of atoms in a chemical formula. Then we can define the volume derivative of bulk modulus at constant mean atomic weight (regardless if the temperature or pressure are constant) as

$$\left(\frac{\partial \ln K_T}{\partial \ln V}\right)_{\overline{M}_a} = -\chi. \tag{A3}$$

Anderson and Nafe (1965) showed that χ is a constant of ~4 for many crystalline oxides and silicates with the same mean atomic weight. For a small range of $\overline{M}$, Eq. (A3) reduces to a linear relationship between the bulk sound velocity and density as demonstrated by Chung (1972)

$$v_K = a(\overline{M}) + b\rho, \tag{A4}$$

where $v_K = (K/\rho)^{1/2}$. Eq. (A4) is the original form of Birch's law proposed by Birch (1961).

Essentially, Birch's law says that the volume dependencies of bulk modulus at constant temperature, pressure, and mean atomic weight are roughly the same, that is

$$K' = \delta = \chi \tag{A5}$$

The similar values of anharmonic parameters K', δ, and χ are confirmed by many experiments (e.g., Anderson et al., 1971; Liebermann and Ringwood, 1973).

APPENDIX B. THERMAL EXPANSIVITY AT HIGH PRESSURE

Thermal expansivity as a function of pressure can be obtained by taking the temperature derivative of Eq. (47)

$$\alpha = \frac{1}{K_T}\left(\frac{\partial P}{\partial T}\right)_V. \tag{A6}$$

where the temperature derivative of $\Phi(f, y_1, y_2)$ is needed. y_1 and y_2 are small in the composition range of this study (<0.03) since the sphere diameters are close to each other. Therefore we can simplify the evaluation of Eq. (A6) by neglecting the temperature dependencies of y_1 and y_2 as

$$\left(\frac{\partial \Phi}{\partial T}\right)_V = f\left(\frac{\partial \Phi}{\partial f}\right)\left(\frac{\partial \ln f}{\partial T}\right)_V = (\Gamma - \Phi)\frac{\partial \ln V_m}{\partial T}, \tag{A7}$$

and

$$\begin{aligned}\left(\frac{\partial \Phi_0}{\partial T}\right)_V &= f_0\left(\frac{\partial \Phi_0}{\partial f_0}\right)\left(\frac{\partial \ln f_0}{\partial T}\right)_V \\ &= (\Gamma_0 - \Phi_0)\left(\frac{\partial \ln \overline{V}_{m0}}{\partial T} - \alpha_0\right),\end{aligned} \tag{A8}$$

where

$$\alpha_0 = \frac{\partial \ln \overline{V}_0}{\partial T} \tag{A9}$$

is the room-pressure thermal expansivity of a liquid. Using Eqs. (A7) and (A8), Eq. (A6) can be reduced to

$$\begin{aligned}\left(\frac{\partial P}{\partial T}\right)_V = \frac{P}{T} + \frac{RT}{\overline{V}}\Bigg[&(1-\xi)\theta(\Gamma - \Phi) - ((\theta_0 - \alpha_0)(\Gamma_0 - \Phi_0) \\ &+ \alpha_0(\mu - 1)\Phi_0)\left(\frac{\overline{V}_0}{\overline{V}}\right)^{\mu-1} \\ &- \omega\Phi + (\xi(\theta_0 - \alpha_0)(\Gamma_0 - \Phi_0) + \omega\Phi_0 \\ &+ \xi(\nu - 1)(\theta_0 - \theta)\Phi_0)\left(\frac{\overline{V}_{m0}}{\overline{V}_m}\right)^{\nu-1}\Bigg],\end{aligned} \tag{A10}$$

where θ and ω are related to the temperature dependence of the volume of spheres

$$\theta \equiv \left(\frac{\partial \ln \overline{V}_m}{\partial T}\right)_{\overline{V}} = \frac{1}{\overline{V}_m}\sum_{i=1}^{m} X_i \overline{V}_{mi}\vartheta_i - \alpha_0\xi, \tag{A11}$$

$$\theta_0 \equiv \left(\frac{\partial \ln \overline{V}_{m0}}{\partial T}\right)_{\overline{V}} = \frac{1}{\overline{V}_{m0}}\sum_{i=1}^{m} X_i \overline{V}_{m0i}\vartheta_i, \tag{A12}$$

and

$$\omega \equiv \left(\frac{\partial \xi}{\partial T}\right)_{\overline{V}} = \frac{1}{\overline{V}_m}\sum_{i=1}^{m} X_i \overline{V}_{mi}\xi_i\vartheta_i - \theta\xi - \alpha_0(\zeta + \xi^2), \tag{A13}$$

with

$$\vartheta_i = \left(\frac{\partial \ln \overline{V}_{m0i}}{\partial T}\right)_{\overline{V}} = \frac{3\eta_i}{T} + \alpha_0\xi_i. \tag{A14}$$

Note that here η_i is defined as the temperature dependence of sphere diameters at constant liquid volume. When temperature changes, the total volume of the liquid also changes due to the thermal expansion. Since the sphere diameters are also volume dependent, the second term on the right hand side of Eq. (A14) thus represents the effect of thermal expansion.

For the case that the deformability of spheres is a linear function of the packing fraction (Eq. (51)), Eq. (A10) remains valid, but θ and ω should be evaluated as

$$\theta = \frac{2\tau f_0 + (1-\xi_0)}{\tau f_0 + (1-\xi_0)}(\theta_0 - \alpha_0) - \frac{\tau f_0(\theta_0-\alpha_0) + (1-\xi_0)(\overline{V}/\overline{V}_0)^{\tau f_0+(1-\xi_0)}\left(\tau f_0(\theta_0-\alpha_0)\ln\left(\frac{\overline{V}}{\overline{V}_0}\right) - (\tau f_0 + (1-\xi_0))\alpha_0\right)}{\tau f_0 + (1-\xi_0)(\overline{V}/\overline{V}_0)^{\tau f_0+(1-\xi_0)}}, \quad \text{(A15)}$$

and

$$\omega = \tau(f\theta - f_0(\theta_0 - \alpha_0)) \quad \text{(A16)}$$

REFERENCES

Agee C. B. (1998) Crystal–liquid density inversions in terrestrial and lunar magmas. *Phys. Earth Planet. Inter.* **107**, 63–74.

Agee C. B. and Walker D. (1993) Olivin flotation in mantle melt. *Earth Planet. Sci. Lett.* **114**, 315–324.

Ai Y. and Lange R. A. (2008) New acoustic velocity measurements on CaO–MgO–Al_2O_3–SiO_2 liquids: reevaluation of the volume and compressibility of $CaMgSi_2O_6$–$CaAl_2Si_2O_8$ liquids to 25 GPa. *J. Geophys. Res.* **113**, B04203.

Andersen H. C., Weeks J. D. and Chandler D. (1971) Relationship between the hard-sphere fluid and fluids with realistic repulsive forces. *Phys. Rev. A* **4**, 1597–1607.

Anderson D. L. (1989) *Theory of the Earth*. Blackwell Scientific Publications.

Anderson D. L., Sammis C. and Jordan T. (1971) Composition and evolution of the mantle and core. *Science* **171**, 1103–1112.

Anderson O. L. (1974) The determination of the volume dependence of the Grüneisen parameter γ. *J. Geophys. Res.* **79**, 1153–1155.

Anderson O. L. (1995) *Equations of State of Solids for Geophysics and Ceramic Science*. Oxford University Press.

Anderson O. L. and Nafe J. E. (1965) The bulk modulus–volume relationship for oxide compounds and related geophysical problems. *J. Geophys. Res.* **70**, 3951–3963.

Angel R. J. (2004) Equations of state of Plagioclase Feldspars. *Contrib. Mineral. Petrol.* **146**, 506–512.

Ashcroft N. W. and Langreth D. C. (1967) Structure of binary liquid mixtures. I. *Phys. Rev.* **156**, 685–692.

Asimow P. D. and Ahrens T. J. (2010) Shock compression of liquid silicates to 125 GPa: the anorthite–diopside join. *J. Geophys. Res.* **115**, B10209. doi:10.1029/2009JB007145.

Baidov V. V. and Kunin L. L. (1968) Speed of ultrasound and compressibility of molten silica. *Sov. Phys. – Dokl.* **13**, 64–65.

Barrat J.-L. and Hansen J.-P. (2003) *Basic Concepts for Simple and Complex Liquids*. Cambridge University Press.

Bass J. D. (1995) Elasticity of minerals, glasses, and melts. In *Mineral Physics and Crystallography: A Handbook of Physical Constants* (ed. T. J. Ahrens). American Geophysical Union, pp. 45–63.

Ben-Amotz D. and Stell G. (2004) Hard sphere perturbation theory for fluids with soft-repulsive-core potentials. *J. Chem. Phys.* **120**, 4844–4851.

Birch F. (1947) Finite elastic strain of cubic crystals. *Phys. Rev.* **71**, 809–824.

Birch F. (1961) The velocity of compressional waves in rocks to 10 kilobars, part 2. *J. Geophys. Res.* **66**, 2199–2224.

Blum L., Vericat F. and Fawcett W. R. (1992) On the mean spherical approximation for hard ions and dipoles. *J. Chem. Phys.* **96**, 3039–3044.

Bockris J. O. M. and Kojonen E. (1960) The compressibilities of certain molten alkali silicates and borates. *J. Am. Ceram. Soc.* **82**, 4493–4497.

Boehler R. and Kennedy G. C. (1977) Pressure dependence of the thermodynamical Grüneisen parameter of liquids. *J. Appl. Phys.* **48**, 4183–4186.

Boehler R. and Ramakrishnan J. (1980) Experimental results on the pressure dependence of the Grüneisen parameter: a review. *J. Geophys. Res.* **85**, 6996–7002.

Bottinga Y. (1985) On the isothermal compressibility of silicate liquids at high pressure. *Earth Planet. Sci. Lett.* **74**, 350–360.

Bottinga Y. and Weill D. F. (1970) Densities of liquid silicate systems calculated from partial molar volumes of oxide components. *Am. J. Sci.* **269**, 169–182.

Brown J. M., Slutsky L. J., Nelson K. A. and Cheng L.-T. (1988) Velocity of sound and equations of state for methanol and ethanol in a diamond-anvil cell. *Science* **241**, 65–67.

Caccamo C. and Malescio G. (1989) Phase stability of dense charged hard sphere fluid mixtures. *J. Chem. Phys.* **90**, 1091–1098.

Chandler D. (1978) Structures of molecular liquids. *Annu. Rev. Phys. Chem.* **29**, 441–471.

Chen G. Q., Ahrens T. J. and Stolper E. M. (2002) Shock-wave equation of state of molten and solid fayalite. *Phys. Earth Planet. Inter.* **134**, 35–52.

Chung D. H. (1972) Birch's law: why is it so good? *Science* **177**, 261–263.

de Koker N. P., Stixrude L. and Karki B. B. (2008) Thermodynamics, structure, dynamics, and freezing of Mg_2SiO_4 liquid at high pressure. *Geochim. Cosmochim. Acta* **72**, 1427–1441.

Egelstaff P. A. (1994) *An Introduction to the Liquid State*. Oxford University Press.

Fei Y. (1995) Thermal expansion. In *Mineral Physics and Crystallography: A Handbook of Physical Constants* (ed. T. J. Ahrens). American Geophysical Union, pp. 29–41.

Fisher M. and Levin Y. (1993) Criticality in ionic fluids: Deby–Huckel theory, Bjerrum, and beyond. *Phys. Rev. Lett.* **71**, 3826–3829.

Funamori N., Yamamoto S., Yagi T. and Kikegawa T. (2004) Exploratory studies of silicate melt structure at high pressures and temperatures by in situ X-ray diffraction. *J. Geophys. Res.* **109**, B03203. doi:10.1029/2003JB002650.

George A. M. and Stebbins J. F. (1998) Structure and dynamics of magnesium in silicate melts: a high-temperature ^{25}MgO NMR study. *Am. Mineral.* **83**, 1022–1029.

Ghiorso M. S. (2004a) An equation of state for silicate melts. I. Formulation of a general model. *Am. J. Sci.* **304**(8–9), 637–678.

Ghiorso M. S. (2004b) An equation of state for silicate melts. III. Analysis of stoichiometric liquids at elevated pressure: shock compression data, molecular dynamics simulations and mineral fusion curves. *Am. J. Sci.* **304**(8–9), 752–810.

Ghiorso M. S. (2004c) An equation of state for silicate melts. IV. Calibration of a multicomponent mixing model to 40 GPa. *Am. J. Sci.* **304**(8–9), 811–838.

Ghiorso M. S. and Sack R. O. (1995) Chemical mass transfer in magmatic processes IV. A revised and internally consistent thermodynamic model for the interpolation and extrapolation of liquid–solid equilibra in magmatic systems at elevated temperatures and pressures. *Contrib. Mineral. Petrol.* **119**, 197–212.

Ghiorso M. S. and Kress V. C. (2004) An equation of state for silicate melts. II. Calibration of volumetric properties at 10^5 Pa. *Am. J. Sci.* **304**(8–9), 679–751.

Ghiorso M. S., Hirschmann M. M., Reiners P. W. and Kress V. C. (2002) The pMELTS: a revision of MELTS for improved calculations of phase relations and major element partitioning related to partial melting of the mantle to 3 GPa. *Geochem. Geophys. Geosyst.* **3**. doi:10.1029/2001GC000217.

Guillot B. and Guissani Y. (1996) Towards a theory of coexistence and criticality in real molten salts. *Mol. Phys.* **1996**, 37–86.

Guillot B. and Sarda P. (2006) The effect of compression on noble gas solubility in silicate melts and consequences for degassing at mid-ocean ridges. *Geochim. Cosmochim. Acta* **70**, 1215–1230.

Hansen J.-P. and McDonald I. R. (2006) *Theory of Simple Liquids*. Academic Press.

Hansen-Goos H. and Roth R. (2006) A new generalization of the Carnahan–Starling equation of state to additive mixtures of hard spheres. *J. Chem. Phys.* **124**, 154506.

Henderson D. (1964) The theory of liquids and dense gases. *Annu. Rev. Phys. Chem.* **15**, 31–62.

Hugh-Jones D. A. and Angel R. J. (1994) A compressional study of $MgSiO_3$ orthoenstatite up to 8.5 GPa. *Am. Mineral.* **79**, 405–410.

Isaak D. G., Ohno I. and Lee P. C. (2006) The elastic constants of monoclinic single-crystal chrome-diopside to 1300 K. *Phys. Chem. Miner.* **32**, 691–699.

Itami T. and Shimoji M. (1980) Hard-sphere model of fused salts. *J. C. S. Faraday II* **76**, 1347–1353.

Karki B. B., Bhattarai D. and Stixrude L. (2006) First-principles calculations of the structural, dynamical, and electronic properties of liquid MgO. *Phys. Rev. B* **73**, 174208.

Karki B. B., Bhattarai D. and Stixrude L. (2007) First-principles simulations of liquid silica: structural and dynamical behavior at high pressure. *Phys. Rev. B* **76**, 104205.

Kress V. C. and Carmichael I. S. E. (1991) The compressibility of silicate liquids containing Fe_2O_3 and the effect of composition, temperature, oxygen fugacity and pressure on their redox states. *Contrib. Mineral. Petrol.* **108**, 82–92.

Kress V. C., Williams Q. and Carmichael I. S. E. (1988) Ultrasonic investigation of melts in the system Na_2O–Al_2O_3–SiO_2. *Geochim. Cosmochim. Acta* **52**, 283–293.

Lange R. A. (1994) The effect of H_2O, CO_2 and F on the density and viscosity of silicate melts. In *Volatiles in Magmas*, vol. 30 (eds. M. R. Carroll and J. R. Holloway). Mineralogical Society of America, pp. 331–369.

Lange R. A. (1997) A revised model for the density and thermal expansivity of K_2O–Na_2O–CaO–MgO–Al_2O_3–SiO_2 liquids from 700 to 1900 K: extension to crustal magmatic temperatures. *Contrib. Mineral. Petrol.* **130**, 1–11.

Lange R. A. and Carmichael I. S. E. (1987) Densities of Na_2O–K_2O–CaO–MgO–FeO–Fe_2O_3–$A1_2O_3$–TiO_2–SiO_2 liquids: new measurements and derived partial molar properties. *Geochim. Cosmochim. Acta* **51**, 2931–2946.

Lange R. A. and Carmichael I. S. E. (1990) Thermodynamic properties of silicate liquids with emphasis on density thermal expansion and compressibility. In *Modern methods of igneous petrology; understanding magmatic processes,*, vol. 24 (eds. J. Nicholls and J. K. Russell). Mineralogical Society of America, pp. 25–64.

Lange R. A. and Navrotsky A. (1992) Heat capacities of Fe_2O_3-bearing silicate liquids. *Contrib. Mineral. Petrol.* **110**, 311–320.

Lebowitz J. L. (1964) Exact solution of generalized Percus–Yevick equation for a mixture of hard spheres. *Phys. Rev.* **133**, A895–A899.

Lebowitz J. L., Helfand E. and Praestgaard E. (1965) Scaled particle theory of fluid mixtures. *J. Chem. Phys.* **43**, 774–779.

Lee S. K., Cody G. D., Fei Y. and Mysen B. O. (2004) Nature of polymerization and properties of silicate melts and glasses at high pressure. *Geochim. Cosmochim. Acta* **68**, 4189–4200.

Levien L., Weidner D. J. and Prewitt C. T. (1979) Elasticity of diopside. *Phys. Chem. Miner.* **4**, 105–113.

Liebermann R. C. and Ringwood A. E. (1973) Birch's law and polymorphic phase transformations. *J. Geophys. Res.* **78**, 6926–6932.

Longuet-Higgins H. C. and Widom B. (1964) A rigid sphere model for the melting of argon. *Mol. Phys.* **8**, 549–553.

Mansoori G. A., Carnahan N. F., Starling K. E. and Leland T. W. (1971) Equilibrium thermodynamic properties of the mixture of hard spheres. *J. Chem. Phys.* **54**, 1523–1525.

March N. H. and Tosi M. P. (2002) *Introduction to Liquid State Physics*. World Scientific Publishing Co. Pte. Ltd.

McBroom R. B. and McQuarrie D. A. (1983) Mean field theory of fused salts. *J. Phys. Chem.* **87**, 3171–3173.

McMillan P. F. and Wolf G. H. (1994) Vibrational spectroscopy of silicate liquids. In *Structure, Dynamics and Properties of Silicate Melts*, vol. 32 (eds. J. F. Stebbins, P. F. McMillan and D. B. Dingwell). Mineralogical Society of America, pp. 247–315.

Miller G. H., Stolper E. M. and Ahrens T. J. (1991) The equation of state of a molten komatiite 1. Shock wave compression to 36 GPa. *J. Geophys. Res.* **96**, 11831–11848.

Mosenfelder J. L., Asimow P. D., Frost D. J., Rubie D. C. and Ahrens T. J. (2009) The $MgSiO_3$ system at high pressure: Thermodynamic properties of perovskite, postperovskite, and melt from global inversion of shock and static compression data. *J. Geophys. Res.* **114**, B01203. doi:10.1029/2008JB005900.

Mysen B. O. and Richet P. (2005) *Silicate Glasses and Melts: Properties and Structure*. Elsevier.

Ohtani E. and Maeda M. (2001) Density of basaltic melt at high pressure and stability of the melt at the base of the lower mantle. *Earth Planet. Sci. Lett.* **193**, 69–75.

Poirier J.-P. (2000) *Introduction to the Physics of the Earth's Interior*. Cambridge University Press.

Reiss H., Frisch H. L. and Lebowitz J. L. (1959) Statistical mechanics of rigid spheres. *J. Chem. Phys.* **31**, 369–380.

Richet P. and Neuville D. R. (1992) Thermodynamics of silicate melts: configurational properties. *Adv. Phys. Geochem.* **10**, 132–161.

Rigden S. M., Ahrens T. J. and Stolper E. M. (1988) Shock compression of molten silicate: results for a model basaltic composition. *J. Geophys. Res.* **93**, 367–382.

Rigden S. M., Ahrens T. J. and Stolper E. M. (1989) High-pressure equation of state of molten anorthite and diopside. *J. Geophys. Res.* **94**, 9508–9522.

Rivers M. L. and Carmichael I. S. E. (1987) Ultrasonic studies of silicate melts. *J. Geophys. Res.* **92**(B9), 9247–9270.

Rosenfeld Y. (1993) Free energy model for inhomogeneous fluid mixtures: Yukawa-charged hard spheres, general interactions, and plasmas. *J. Chem. Phys.* **98**, 8126–8148.

Rowlinson J. S. (1964) The statistical mechanics of systems with steep intermolecular potentials. *Mol. Phys.* **8**, 107–115.

Schilling F. R., Sinogeikin S. V., Hauser M. and Bass J. D. (2003) Elastic properties of model basaltic melt compositions at high temperatures. *J. Geophys. Res.* **108**(B6), 2304. doi:10.1029/2001JB000517.

Secco R. A., Manghnani M. H. and Liu T.-C. (1991) The bulk modulus–attenuation–viscosity systematics of diopside–anorthite melts. *Geophys. Res. Lett.* **18**, 93–96.

Shankland T. J. (1972) Velocity–density systematics: derivation from Debye theory and the effect of ionic size. *J. Geophys. Res.* **77**, 3750–3758.

Shimoda K. and Okuno M. (2006) Molecular dynamics study of $CaSiO_3$–$MgSiO_3$ glasses under high pressure. *J. Phys.: Condens. Matter* **18**, 6531–6544.

Smyth J. R. and McCormick T. C. (1995) Crystallographic data for minerals. In *Mineral Physics and Crystallography: A Handbook of Physical Constants* (ed. T. J. Ahrens). American Geophysical Union.

Stebbins J. F. (1995) Dynamics and structure of silicate and oxide melts: nuclear magnetic resonance studies. In *Structure, dynamics and properties of silicate melts*, vol. 32 (eds. J. F. Stebbins, P. F. McMillan and D. B. Dingwell). Mineralogical Society of America, pp. 191–246.

Stillinger F. H. (1961) Compressibility of simple fused salts. *J. Chem. Phys.* **35**, 1581–1583.

Stixrude L. and Karki B. (2005) Structure and freezing of $MgSiO_3$ liquid in Earth's lower mantle. *Science* **310**, 297–299.

Stixrude L. and Lithgow-Bertelloni C. (2005) Thermodynamics of mantle minerals – I. Physical properties. *Geophys. J. Int.* **162**, 610–632.

Stixrude L., de Koker N. P., Sun N., Mookherjee M. and Karki B. B. (2009) Thermodynamics of silicate liquids in the deep Earth. *Earth Planet. Sci. Lett.* **278**, 226–232.

Suski L. and Tomczyk P. (1981) Application of hard-sphere theory to the compressibilities of some fused-salt binary mixtures. *J. Chem. Thermodyn.* **13**, 803–814.

Suzuki A. and Ohtani E. (2003) Density of peridotite melts at high pressure. *Phys. Chem. Miner.* **30**, 449–456.

Suzuki A., Ohtani E. and Kato T. (1998) Density and thermal expansion of a peridotite melt at high pressure. *Phys. Earth Planet. Inter.* **107**, 53–61.

Tenner T. J., Lange R. A. and Downs R. T. (2007) The albite fusion curve re-examined: new experiments and the high-pressure density and compressibility of high albite and $NaAlSi_3O_8$ liquid. *Am. Mineral.* **92**, 1573–1585.

Thiele E. (1963) Equation of state for hard spheres. *J. Chem. Phys.* **39**, 474–479.

Tomczyk P. (1977) Compressibility of simple molten salts. *J. Phys. Chem.* **81**, 183–184.

Vinet P., Ferrante J., Smith J. R. and Rose J. H. (1986) A universal equation of state for solids. *J. Phys. C: Solid State Phys.* **19**, L467–L473.

Wang H. (1989) *Elasticity of Silicate Glasses*. M.S., University of Illinois at Urbana.

Webb S. and Courtial P. (1996) Compressibility of melts in the $CaO–Al_2O_3–SiO_2$ system. *Geochim. Cosmochim. Acta* **60**(1), 75–86.

Wertheim (1963) Exact solution of the Percus–Yevick integral equation for hard spheres. *Phys. Rev. Lett.* **10**, 321–323.

Wolf G. H. and McMillan P. F. (1995) Pressure effects on silicate melt structure and properties. In *Structure, Dynamics and Properties of Silicate Melts*, vol. 32 (eds. J. F. Stebbins, P. F. McMillan and D. B. Dingwell). Mineralogical Society of America, pp. 505–561.

Xue X., Stebbins J. F., Kanzaki M. and Tronnes R. G. (1989) Silicon coordination and speciation changes in a silicate liquid at high pressures. *Science* **245**, 962–964.

Yamada A., Inoue T., Urakawa S., Funakoshi K.-i., Funamori N., Kikegawa T., Ohfuji H. and Irifune T. (2007) In situ X-ray experiment on the structure of hydrous Mg–silicate melt under high pressure and high temperature. *Geophys. Res. Lett.* **34**, L10303. doi:10.1029/2006GL028823.

Zhou Y. and Stell G. (1995) Criticality of charged systems. II. The binary mixture of hard spheres and ions. *J. Chem. Phys.* **102**, 5796–5802.

Zhou Y., Yeh S. and Stell G. (1995) Criticality of charged systems. I. The restricted primitive model. *J. Chem. Phys.* **102**, 5785–5795.

Associate editor: Bjorn Mysen